# The nyerereite crystal structure: a possible messenger from the deep Earth.

Azzurra Zucchini 1*, Pavel N. Gavryushkin 2,3, Alexander V. Golovin 2, Nadezhda B. Bolotina 4, Paola Stabile 5, Michael Robert Carroll 5, Paola Comodi 1, Francesco Frondini 1, Daniele Morgavi 1, Diego Perugini 1, Fabio Arzilli 6, Marco Cherin 1, Emmanuel Kazimoto 7, Konstantin Kokh 2,3,8, Artem Kuznetsov 2, Inna V. Medrish 9

1 Department of Physics and Geology, University of Perugia, 06123 Perugia, Italy;

2 Sobolev Institute of Geology and Mineralogy, Siberian Branch of Russian Academy of Sciences, 630090 Novosibirsk, Russia;

3 Novosibirsk State University, Novosibirsk 630090, Russia;

4 Shubnikov Institute of Crystallography, Federal Scientific Research Centre 'Crystallography and Photonics' of Russian Academy of Sciences, Leninskii prosp. 59, 119333 Moscow, Russian Federation;

5 School of Science and Technology, Geology Division, University of Camerino, 62032 Camerino, Italy;

6 School of Earth and Environmental Sciences, University of Manchester, M139PL, Manchester, UK;

7 Department of Geosciences, School of Mines and Geosciences, University of Dar es Salaam 16103, Uvumbuzi Rd, Dar es Salaam Tanzania;

8 Kemerovo State University, 6 Krasnaya Str., Kemerovo, 650000, Russia.

9 Samara Center for Theoretical Material Science (SCTMS), Samara State Technical University, Molodogvardeyskaya St. 244, Samara, Russia 443100

(*correspondence: azzurra.zucchini@unipg.it)

## Abstract

Carbonates in the system $Na_2CO_3$–$CaCO_3$ are nowadays suggested as having a wide stability field at conditions of the mantle transition zone. The proposed analysis of nyerereite crystal structure, that have limited stability fields at ambient conditions, and its similarities with already known carbonates stable at high pressure conditions, allowed to propose that nyerereite likely undergoes phase transition at both high-pressure/high-temperature conditions supporting the hypothesis that it takes part in the carbon transportation from the mantle/deep crust towards the surface with important implication for the deep carbon cycle associated with carbonatites.

K-free nyerereite [$Na_2Ca(CO_3)_2$] was synthesized both at hydrothermal conditions and from the melt. The crystal structure of nyerereite was here refined as a three-component twinned structure in the centrosymmetric *Pbca* space group with ratio of the three twinning components 0.221(3):0.287(3):0.492(3). Twinning at micro- and nano- level can introduce some minor structural deformations that influence the likely occurrence of the inversion center as one of the symmetry elements in nyerereite crystal structure. Based on the automated topological algorithms we show that nyerereite has the unique crystal structure, not having analogues among the known crystal structures, except for the structure with similar composition $K_2Ca(CO_3)_2$ - fairchildite.

A comparison between the centrosymmetric *Pbca* nyerereite structure and that of aragonite ($CaCO_3$, *Pmcn* space group) is proposed and two main scenarios arises for the high pressure form of $Na_2Ca(CO_3)_2$: (1) polysomatic relations as the interlayering of the high pressure polymorph $Na_2CO_3$ and $CaCO_3$ - aragonite, and (2) high pressure crystal structure with 9-fold coordinated Na and Ca sites resembling that of aragonite. The proposed discussion heightens the interest in the baric behavior of the nyerereite structure and strengthens the hypothesis about the possibility for the nyerereite crystal structure to be stable at high pressure/high temperature conditions.

**Keywords:** Nyerereite, single-crystal X-ray diffraction, hydrothermal synthesis, melt crystallization, Raman spectroscopy, alkali-carbonates.

## Introduction

The ubiquitous occurrence of Ca-Mg carbonates on Earth comes together with an intriguing paucity of alkaline and earth-alkaline carbonatites in the $CaCO_3$-$(Na,K)_2CO_3$ system likely due to their ephemeral behavior. Minerals such as nyerereite [approximate chemical formula $(Na_{1.64}K_{0.36})Ca(CO_3)_2$ (Bolotina et al., 2017)] and gregoryite [$(NaCa_xK)_{2-x}CO_3$], at ambient conditions and in presence of meteoric water, rapidly transforms to the end-members Ca-carbonatite rocks (Gavryushkin et al. 2016), through intermediate stages such as pirssonite-like structures [$Na_2Ca(CO_3)_2 \cdot 2(H_2O)$] (Zaitsev and Keller, 2006; Zaitsev et al., 2008; Stoppa et al. 2009 and references therein). The transformation is quite rapid, occurring over a few months to a couple of years (Zaitsev and Keller, 2006).

### Alkali-carbonates in the geological record

Alkaline carbonatite magmas are of great interest because they may represent partial melts produced at significantly lower mantle melting temperatures compared with basaltic magmas (e.g. Golubkova et al. 2015) and they may represent a powerful agent promoting mantle metasomatism (Rosatelli et al., 2007). Different geological settings host carbonatites, including intra-plate magmatism in continental areas and along continental rifts (Mattsson et al. 2018 and references therein) raising important questions on the geodynamic significance of carbonatite magmatism.

The only active carbonatite volcano on the Earth, erupting significant amount of natrocarbonatite magmas ($Na_2O + K_2O \sim 40$ wt%, Keller and Zaitsev, 2012), is the Oldoinyo Lengai volcano (East African Rift System, northern Tanzania). The erupted products are

predominantly composed of phonolitic and nephelinitic pyroclasts and lesser amounts of lava flows (Mattsson et al. 2018). The carbonatite lavas present the lowest temperature (>600 °C) and the lowest viscosity (Krafft and Keller, 1989; Dawson, et al., 1990; Oppenheimer, 1998) and the main rock-forming minerals of these natrocarbonatites are (orthorhombic) nyerereite and gregoryite (e.g. McKie and Frankis, 1977; Peterson, 1990; Zaitsev et al., 2009; Mitchell and Kamenetsky, 2012).

One of the most interesting occurrences of Na-Ca carbonates is in mantle-derived melt inclusions, which pose important constraints to the composition and origin of kimberlites and mantle-derived melts and provide information on the nature of primary melts and deep Earth composition (Sharygin et al., 2017; Giuliani et al., 2020).

Nyerereite-like carbonates were identified as daughter minerals within primary/secondary melt inclusions in rock-forming minerals of kimberlites from Udachnaya-East, Gahcho Kué, Jericho, Aaron, Leslie, Koala, Roger, Monastery, Bultfontein pipes, Majuagaa dike, Mark kimberlite hypabyssal body and Benfontein kimberlite sill complex (e.g. Golovin et al., 2003, 2007, 2017a; Kamenetsky et al., 2009, 2013; Giuliani et al., 2017; Abersteiner et al., 2018a, 2018b, 2019, 2020). These kimberlite emplacements are located practically within all worldwide ancient cratons. Moreover, nyerereite-like carbonates were found among the daughter minerals within high-pressure mantle origin primary/secondary carbonatite melt inclusions in minerals of the mantle xenoliths from kimberlites Bultfontein and Udachnaya-East pipes (Giuliani et al., 2012; Golovin et al., 2017a, 2018, 2020) and even as minerals from multiphase solid inclusions in diamonds from the Juina area, Brazil (Kaminsky et al., 2009).

A further example is the kamafugite-melilitite-carbonatite lime-rich igneous rocks outscopping in the italian Umbria-Latium ultra-alkaline province and the Intramontane Ultra-alkaline province (Panina et al., 2003; Isakova et al., 2017; Isakova et al., 2019). In this area, nyerereite, in the form of crystalline inclusions, was identified in the minerals of rocks from Vulture

(Stoppa et al., 2009), as well as in other alkaline volcanic complexes around the world, e.g. Kerimasi (Zaitsev, 2010), and Tinderet (Zaitsev et al., 2013), from the Guli pluton (Kogarko et al., 1991) and in minerals of the Afrikanda ultramafic–alkaline complex (Zaitsev and Chakhmouradian, 2002).

Nyerereite is also present as a daughter mineral within melt inclusions in minerals from the Gardiner and Kovdor carbonatite-bearing ultramafic alkaline complexes (Veksler et al., 1998; Sokolov et al., 2006), calcite-rich carbonatites from the Oka carbonatite complex (Chen et al., 2013), carbonatitic lavas in Catanda (Campeny et al., 2015) and calciocarbonatite and jacupirangite from Kerimasi volcano (Guzmics et al., 2011; Káldos et al., 2015).

## Nyerereite crystal structure and open questions

The crystal structure solution of nyerereite has been the subject of several studies (e.g. Frankis and McKie 1973, Gavryushkin et al. 2016, Bolotina et al., 2017). Difficulties in the final solution of the nyerereite crystal structure were overcome by using K-free synthetic samples (Frankis and McKie, 1973; Gavryushkin et al., 2016; Song, 2017) where incommensurate modulation is not present (Frankis and McKie, 1973; Gavryushkin et al., 2016; Bolotina et al., 2017). Synthetic nyerereite showed good crystallinity and the crystal structure was refined as a three-component orthorhombic twins with either $P2_1ca$ (Gavryushkin et al., 2016) (Figure S1 deposited in the *Supplemental Materials* section) or *Pbca* (Song et al., 2017) space groups (Figure S2 deposited in the *Supplementary Materials* section). Two high temperature phase transitions were observed in nyerereite starting from the room temperature structure ($\alpha$-nyerereite) towards (i) $\beta$-nyerereite (*Cmcm* space group; Gavryushkin et al., 2016) in the *T* range 292°C (natural sample) - 400°C (synthetic sample) and (ii) $\gamma$-nyerereite ($P6_3/mmc$ symmetry; Gavryushkin et al., 2016) in the *T* range 340°C (natural sample) - 445°C (synthetic sample) (Johnson and Robb, 1973; Evans and Milton, 1973; McKie and Frankis, 1977).

Analogously to fairchildite [high *T* form of $K_2Ca(CO_3)_2$], oxygens in $\gamma$-nyerereite are expected to be disordered (Gavryushkin et al., 2016; Pertlik, 1981).

Besides the hydrothermal synthesis, other techniques have been adopted to synthesize $Na_2Ca(CO_3)_2$ crystals, namely, thermally induced solid-state reaction of $Na_2CO_3$ + $CaCO_3$ (Smith et al., 1971) and dehydration of mineral gaylussite [$Na_2Ca(CO_3)_2$•$5(H_2O)$] (Evans and Milton, 1973; Johnson and Robb, 1973).

In the present work we consider different synthesis conditions, namely hydrothermal synthesis and synthesis from the melt, the latter one employed to obtain a new type of nyerereite samples that resembles the natural samples observed in melt inclusions of kimberlites. The synthetic alkali-carbonates mixtures are studied by a multimethodological approach, namely, scanning electron microscopy (SEM) and energy dispersive spectroscopy (EDS), Raman spectroscopy and single crystal X-ray diffraction (SC-XRD) with a particular focus on the structure solution of nyerereite, showing that it can be centrosymmetric or not, depending on conditions of crystallization

Despite the well-known high-pressure behavior of Ca-Mg-Fe carbonates(e.g., Zucchini et al., 2014, 2017; Merlini et al., 2012, 2016; Cerantola et al., 2017), the Na-Ca phase stability at mantle/deep crust conditions is poorly known and experimental and theoretical studies have been limited to minerals other than nyerereite (Borodina et al., 2018; Vennari et al., 2018; Rashchenko et al., 2020). The only exception is the high-pressure (H*P*) Raman study of nyerereite made by Rashchenko et al. (2017) where, however, the analyzed *P* range (up to 6.4 GPa) and the lack of crystal structure data did not allow the characterization of the minor structural observed deformations that occurred at 0.5 and 3.0 GPa, that were speculatively ascribed to rearrangement of the $CO_3^{2-}$ groups in the nyerereite crystal structure.

The proposed analysis of nyerereite crystal structure, that have limited stability at low pressures and temperatures, and the study of its similarities with already known carbonates, stable at H*P*

conditions, allowed to propose that nyerereite likely undergoes phase transition at both H*P* and high-temperature (H*T*) conditions that could stabilize them down to the mantle transition zone, supporting the hypothesis that these minerals take part in the carbon transportation from the mantle/deep crust towards the surface with important implication for the deep carbon cycle associated with carbonatites.

## Materials and methods

### Synthesis

**Hydrothermal synthesis.** Hydrothermal synthesis of nyerereite was performed, following the procedure described in Frankis and McKie (1973), in water-pressurized cold seal pressure vessels (Nimonic 105) at the Department of Geology at University of Camerino (Italy). The starting material was prepared from a mixture of dried carbonates, $Na_2CO_3$ (60mole%) and $CaCO_3$ (40mole%). The mixture was first homogenized and mixed in an agate ball mill for 30 min before the capsule preparation. The powder material (~15 mg per experiment) along with ca. 10ml of distilled water was then loaded into Au capsules (with dimensions of 25mm length, 3mm inner diameter, 3.4mm outer diameter). The capsules were weighed after each addition of material and then sealed by welding. Weight after welding was checked to verify that water was not lost during welding. The intrinsic redox condition of the CSPV apparatus is close to NNO +0.8 (Di Matteo et al., 2004; Fabbrizio et al., 2006; Fabbrizio and Carroll, 2008; Stabile et al., 2018, 2020). Temperature was measured in the sample position with a K-type thermocouple with an accuracy of ±5°C. Pressure was monitored by a high-pressure transducer or Bourdon-tube pressure gauges, considered accurate to ±2 MPa (Arzilli et al., 2020). The samples were heated and pressurized to reach the experimental temperature of 550°C and pressure of 100 MPa. Experiments lasted 15 days (hereafter NHD15) and the samples were

quenched from experimental conditions to room conditions by removing the bomb from the furnace and immersing it in a high-pressure stream of compressed air, providing a cooling rate of ~120°C/min. For all the samples run, the quench was isobaric as pressure was maintained constant during cooling by using a large volume pressure reservoir and a hand operated pressure generator.

**Synthesis from the melt.** $Na_2Ca(CO_3)_2$ crystals (hereafter NMAG) were obtained by slow cooling of the stoichiometric melt in a vertical vitreous graphite crucible. The crucible with a mixture of $CaCO_3$ and $Na_2CO_3$ was placed in a quartz reactor, which was continuously purged with nitrogen gas. Heating was carried out by a resistive heating furnace up to 850°C. There was a minimum temperature at the crucible's bottom, which ensured directional crystallization from bottom to top with a decrease in temperature at a rate of 1 deg/hour.

**SEM – EDS**

Analyses were obtained at the Analytical Centre for Multielemental and Isotope Research of Siberian Branch of the Russian Academy of Science (Sobolev Institute of Geology and Mineralogy, Novosibirsk, Russia). The analyses of hydrothermal and magmatic synthetic nyerereite and back-scattering electron (BSE) images were obtained by a Tescan MIRA3 LMU scanning electron microscope equipped with an Aztec Energy X-Max 50+ energy-dispersive X-ray microanalysis system. An accelerating voltage of 20 keV and a beam current of 1.44 nA were used. Spectrum acquisition live time was 35 s. Matrix correction was performed with the XPP algorithm. Pure cobalt was measured to control the probe current and the energy shift.

**Raman spectroscopy**

Raman point measurements (from 0 to 4000 $cm^{-1}$) of individual grains and mixtures of compounds were performed using a LabRAM HR800 dispersive Raman spectrometer using

the excitation line of a 532-nm Nd:YAG laser. In all measurements, a laser power of approximately 10 mW was employed. The scattered Raman light was analyzed with a CCD detector after being dispersed by a grating of 1800 grooves $mm^{-1}$. A 100× lens with a numerical aperture of 0.9 was used on a BX-51 microscope. The frequency was calibrated using the first-order Si line at 520.6 $cm^{-1}$. The wavenumbers are accurate to ±1 $cm^{-1}$.

In experiments on nyerereite synthesized from the melt, single crystals were cut and polished in one direction, therefore, they have the same spectra (the same ratio of the intensity of the Raman lines relative to each other) at different points of the sample.

**SC-XRD**

Optically clear single nyerereite crystals (approximately 20x20x50 $\mu m^3$ in NMAG and 50x50x100 $\mu m^3$ in NHD15) were separated from the synthesis run products and analyzed at room temperature at the University of Perugia (Italy) by using an Oxford Diffraction Xcalibur diffractometer with CCD detector and MoKα radiation (λ = 0.7107 Å). Detector distance to the sample was ca. 66 mm with pixel size ca. 60 μm.

Rotation pictures and 360° φ-scans allowed us to control the crystal quality and optimize the data collection parameters, respectively. Measurements were carried out in a ω-scan mode with 1.0° scan width and 15 s exposure time. The resolution of data collection was set to $\sin\theta/\lambda = 0.72$ $Å^{-1}$.

Data reduction was performed by means of CrysAlisPro software (Agilent Technologies UK Ltd, Yarnton, England.) and an empirical absorption correction was applied by the ABSPACK module as implemented in CrysAlisPro software (Oxford Diffraction/Agilent Technologies).

Refinements were carried out by means of the SHELXLE (Hübschle et al., 2011) in both $P2_1ca$ and *Pbca* space groups, with anisotropic displacement parameters. In Figure S3 (*Supplemental materials*), the collected data extraction and the unit cell used for reflection indexing are shown

226 together with the evidence of the three-component domains rotated of ca. 120° around the *c*
227 axis.

228 In both space groups twinning was introduced following the twinning matrix:

229 $$\left[-\frac{1}{2}\ 1\ 0\ \ -\frac{3}{4}\ -\frac{1}{2}\ 0\ 0\ 0\ 1\right]$$

230

231 **Topological analysis**

232 The topological analysis was performed by means of ToposPro (http://topospro.com), with the
233 aim to search for the topological analogues of the nyerereite crystal structure, through the whole
234 Inorganic Crystal Structure Database (ICSD, release 2020/2) (Blatov et al., 2014). Hereafter,
235 we use three-letter bold symbols of the Reticular Chemistry Structure Resource nomenclature
236 (see Reticular Chemistry Structure Resource at http://rcsr.anu.edu.au/) (O'Keeffe et al., 2008)
237 or *ToposPro N*D*k-n* symbols (Alexandrov et al., 2011) to designate the topological types of the
238 underlying nets. Further details on the used procedure are given in the Supplementary material
239 section together with the obtained results.

240

241 **Results**

242 The synthesis experiments performed in this work were successful and we were capable of
243 recovering several milligrams of sample from each experiment. The run products coming out
244 from the hydrothermal samples have already been characterized by Fastelli et al. (2021).
245 Reflected light images and backscattered electrons (BSE) images of the NHD15 and NMAG
246 samples are shown in Figure 1 and Figure 2 where the lightest regions were attributed, by
247 means of SEM-EDS chemical analysis, to nyerereite with averaged chemical formula
248 $Na_{1.996(5)}Ca_{1.017(3)}(CO_3)_2$ and $Na_{1.996(7)}Ca_{1.002(4)}(CO_3)_2$ for NHD15 and NMAG, respectively.
249 The single point chemical analyses are given in the *Supplemental Material* sections as Table
250 S1. The dark portions in Figures 1 and 2 are attributed to a mixture mainly consisting of $Na_2CO_3$

(Figure 2), with minor amounts of Na-Ca carbonates, together with unreacted $CaCO_3$ grains in NMAG. In *Supplemental material* section backscattered electrons (BSE) images and EDS X-ray maps recorded on selected portions of NMAG and NHD15 are given (Figure S4).

The synthesis run products showed the occurrence of differently shaped nyerereite crystals. On the one hand, NMAG shows acicular nyerereite crystals ranging from a few microns up to a few tens of microns (Figure 2a), strongly interconnected with the $Na_2CO_3$ matrix. On the other hand, in NHD15, nyerereite appears as globular aggregates of rounded crystals with maximum dimensions of approximately 120-150 μm (Figure 2b).

**Syntheses products**

Raman spectra for individual differently oriented nyerereite grains were collected in the range from 0 to 2000 $cm^{-1}$. No differences were observed by comparing them with Golovin et al. (2017b) data (Figure 3), showing the highest peaks at 1073 and 1087 $cm^{-1}$ (± 1 $cm^{-1}$).

Besides the occurrence of nyerereite, additional signals are present in the NHD15 and MNAG Raman spectra (Figure 4). A strong line at 1070 $cm^{-1}$ is present in both NHD15 and NMAG (Figure 4c) that might be related to the presence of thermonatrite ($Na_2CO_3 \cdot H_2O$) together with the peaks at 687 $cm^{-1}$ + 702 $cm^{-1}$ (Figure 4b) and 2972 $cm^{-1}$ + 3254 $cm^{-1}$ (Figure 4d) (Jentzsch et al. 2013, Frezzotti et al. 2012, Frost et al. 2009) in agreement with results from Fastelli et al. (2021). Additional peaks occur at 1079 $cm^{-1}$ + 1082 $cm^{-1}$ (Figure 4c) as well as at 699 $cm^{-1}$ (Figure 4b) that can be attributed to the γ-$Na_2CO_3$ phase (Shatskiy et al., 2013, 2015), whose presence was also observed by Gavryushkin et al. (2016) and Fastelli et al. (2021) in their synthesis run products.

An unassigned peak at approximately 134 $cm^{-1}$ in Figure 4a belongs neither to any of the likely occurring phases (nyerereite, γ-natrite, thermonatrite), nor to plausible occurring phases in the $Na_2CO_3$ – $CaCO_3$ series checked by a comparison with data stored in the RUFF database

(Lafuente et al. 2016) as well as with data from literature (Golovin et al. 2017b). Thus, this might be the signal that an unknown phase in the $Na_2CO_3$ – $CaCO_3$ series is present in the synthesized sample. However, given the very fine intergrowth of the additional phases with $Na_2Ca(CO_3)_2$ in the mix region (Figure 2), it is impossible to get both SC-XRD and Raman spectra from the individual grain. Further studies are needed to truly define the phase assemblage present in the mix region, but is beyond the scope of the present work.

**Nyerereite structure**

The nyerereite structure refinements in both $P2_1ca$ and *Pbca* space groups were satisfactory in terms of the agreement parameters R1 (<0.07) and wR2 (<0.16) as well as GooF (~1). A three-component twinned structure rotated of ca. 120° around the *c* axes was refined in both space groups. However, in $P2_1ca$ too many correlations between atomic coordinates were observed, meaning that corresponding atoms are symmetry equivalent. Thus, we can definitely recommend *Pbca* as the space group for both hydrothermal and magmatic nyerereite, in agreement with results of Song et al. (2017). The ratio of the three twinning components is refined as 0.221(3):0.287(3):0.492(3). The details of data collection and refinement, together with the crystal structure data, can be found in the CIF file (deposited) for both HND15 and NMAG samples. Bond lengths and polyhedral volumes are given in Table S2 as *Supplemental Material*.

In Gavryushkin et al. (2016), where a different hydrothermal synthesis was proposed (partial replacement of $Na_2CO_3$ with NaOH as starting materials), a higher number of reflections broke the reflection conditions of *Pbca* space group in their hydrothermal synthetic samples, with respect to the non-centrosymmetric space group $P2_1ca$. The refined ratio of the twin components showed a nearly identical amount being 0.3363(4):0.3446(4):0.3191(4). Thus, the observed difference in space groups is not an artefact of the refinement, but shows real

difference in the crystal structures, attributed to the different growth conditions, suggesting that nyerereite can have different space groups and twinning at micro- and nano- level, which can introduce some minor structural deformations that inhibit the occurrence of an inversion center.

**Topological analysis.** Our topological analysis suggests that nyerereite is characterized by a unique topology, which does not have analogues in ICSD database except for the structure with similar composition $K_2Ca(CO_3)_2$ (fairchildite), although the subnets of the separate atoms constituting the structure are relatively widespread among carbonates and carbides. 738 crystal structures of borates with stoichiometry similar to that of nyerereite were found in ICSD, however they are all quite different from nyerereite. Among four double carbonates in the system $Na_2CO_3$-$CaCO_3$ [nyerereite, shortite, $Na_2Ca_3(CO_3)_4$ and $Na_4Ca(CO_3)_3$], only $Na_2Ca_3(CO_3)_4$ (Gavryushkin et al, 2014) and $Na_4Ca(CO_3)_3$ (Rashchenko et al, 2018) have analogues among borates. Detailed results of the topological analysis of nyerereite are given in the *Supplemental Material* sections.

**Polyhedra distortion and bond-valences calculation.** The polyhedral distortion index (D) (Table S2, *Supplemental material*) and the bond valence sum (BVS) (Table S3, *Supplemental material*) calculated following the values given by Brese and O'Keeffe (1991) were obtained based on bond lengths as defined by Baur et al. (1974) and implemented using the open-source crystallographic software VESTA (Momma and Izumi, 2011). As regards the carbonate group, on the one hand, the pseudo-planar triangle in C1 is quite regular with the three bond-valences that almost equal each other as in aragonite. The bond-valence of the three carbonate-oxygen bonds has values in the range 1.32-1.34 both in aragonite and nyerereite with coefficient of variation (CV), *i.e.* ratio of the standard deviation to the mean, of approximately 1-2% and a deviation from planarity of 1.9° in NHD15 and 1.2° in NMAG (Table S2).

As regards the C2 site, the bond valences of the three (C-O) bonds are in the range 1.30-1.38 (CV ~ 3%) and the deviation from planarity is 3.2° in NHD15 and 2.5° in NMAG. The (C2-

O4) bond-valence is the highest (1.38) with respect to the other C-O bonds likely due to the high strength of the (Na1-O4) bond (bond valence = 0.22) and the low strength of both the (Na2-O6) and (Na1-O5) bonds being the bond valence 0.16 and 0.05, respectively. Figure 6 shows the atomic structure and bond length/strength.

## Discussion

In all experiments, in addition to the "pure" $Na_2Ca(CO_3)_2$ nyerereite, a mixture consisting mainly of thermonatrite and γ-$Na_2CO_3$ was observed. In the $Na_2CO_3$:$CaCO_3$ range tested by our experiments ($Na_2CO_3$:$CaCO_3$ = 0.6:0.4 in NHD15, $Na_2CO_3$:$CaCO_3$ = 0.7:0.3 in NMAG), results are in agreement with Cooper et al. (1975). Given the ephemeral behavior of both natrite and nyerereite, the occurrence of anhydrous/hydrated $Na_2CO_3$ is not surprising and likely due to the interaction with atmospheric humidity and the handling during sample preparation that led to the formation of $Na_2CO_3 \cdot H_2O$. However, the crystal structure of nyerereite in both NHD15 and NMAG syntheses was here well refined as a three-component twinned structure in the centrosymmetric *Pbca* space group.

The performed topological analysis indicates that there are no strict analogies between the crystal structure of nyerereite and other carbonates except for the structure with similar composition $K_2Ca(CO_3)_2$ (fairchildite). In addition, we observe that double carbonates with simple stoichiometry as nyerereite ($Na_2CO_3$*$CaCO_3$) have no analogues among borates. However, an interesting comparison between the crystal structure of the centrosymmetric *Pbca* nyerereite structure and that of aragonite ($CaCO_3$, *Pmcn* space group) is proposed (Figure 7). The *a* and *c* axes are doubled in nyerereite with respect to aragonite (*a* = 4.96 Å, *b* = 7.97 Å, *c* = 5.74 Å; Antao and Hassan 2009), due to the presence of Na in the mineral crystal structure with the consequent inclination of the $C(2)O_3^{2-}$ groups, lying in the cavities occurring between two Na-layers, of approximately 58° with respect to the (*ab*) plane. A second set of carbonate

groups [$C(1)O_3^{2-}$] lie in the (*ab*) plane, parallel to the Ca-layer, and is less distorted with respect to the former ($D_{C1}$ = 0.002 - 0.004 and $D_{C2}$ = 0.004 - 0.006, Table S2).

The Ca polyhedra in nyerereite has a distortion index close to that of aragonite ($D_{Ca\text{-}nyerereite}$ = 0.03, Table S2; $D_{Ca\text{-}aragonite}$ = 0.025; Antao and Hassan, 2009).

Notwithstanding the bond-valence requirements are respected in the *Pbca* nyerereite (Table S3 in *Supplemental material*) with the bond length scheme previously defined by Gavryushkin et al. (2016), the observed differences in the bong-strengths within Na1 and Na2 polyhedra give rise to their observed higher distortion with respect to the Ca polyhedron ($D_{Na\text{-}nyerereite}$ = 0.05-0.07, Table S2) as well as to the marked deviation from planarity of the C2 atom and tilting of the $C(2)O_3^{2-}$ groups.

By the presented scenario, both Na1 and Na2 polyhedra are supposed to regularize with increasing pressure by likely including in their geometry additional oxygens and increasing their coordination number according to Prewitt and Downs (1998), as already observed in both carbonate and non-carbonate minerals, e.g., dolomite [$CaMg(CO_3)_2$] (Merlini et al., 2012; Zucchini et al., 2014) and galenobismutite ($PbBi_2S_4$) (Comodi et al. 2019). This could drive the *Pbca* nyerereite towards a crystal structure with 9-fold coordinated Na and Ca sites resembling that of aragonite at elevated pressure.

A second scenario might be proposed, based on the polysomatic relation of $Na_2Ca(CO_3)_2$ structures with the structures of γ-$Na_2CO_3$ and $CaCO_3$ calcite (Bolotina et al, 2017). We suggest that some similar polysomatic relations will be preserved in the H*P* from of $Na_2Ca(CO_3)_2$ and it can be presented as the interlayering of H*P* polymorphs $Na_2CO_3$-$P2_1/m$ (Gavryushkin et al. 2016, 2019) and $CaCO_3$ in the form of aragonite. It is worth noting that aragonite was found as an inclusion in mantle olivine from carbonatite tuffs in a leucitite lava flow in Calatrava (Spain) providing evidences for a likely sublithospheric mantle origin for alkaline ultramafic magmas and extrusive carbonatites (Humphreys et al., 2010). The solubility of Na in the structure of

aragonite might be drastically increased through the formation of nano lamellae of H*P* polymorph of $Na_2Ca(CO_3)_2$ giving rise to what has been recently called "Na-aragonite" (Rashchenko et al., 2020). Our hypothesis about formation of modular structures between the H*P* form of $Na_2CO_3$ and aragonite at H*P* is supported by the amount of dissolved $Ca^{2+}$ in the structure of $Na_2CO_3$ up to 15% (Podborodnikov et al., 2018), which cannot be explained with isomorphism as the authors suggested.

The proposed hypotheses are consistent with recent studies on the H*P* behavior of Na-Ca carbonates (Grassi and Schmidt, 2011; Kiseeva et al., 2013; Litasov et al., 2013 Borodina et al., 2018; Vennari et al., 2018; Rashchenko et al., 2020) that have already suggested an important variety of Na-Ca double carbonates in the system $Na_2CO_3$–$CaCO_3$ at H*P*-H*T*, linked each other by a sequence of decomposition reactions (Rashchenko et al., 2020), as well as the existence of high-pressure polymorphs of $Na_2Ca_2(CO_3)_3$-shortite. As a consequence, the stability/decomposition reactions occurring in the mentioned phases during decompression are a fundamental constraint for the $CO_2$ release from mantle-derived magma, which can be expected to influence magma viscosity and eruption explosivity (Allison et al., 2021). If confirmed, the proposed scenarios might confer a role to nyerereite in the carbon transportation within the Earth's mantle, and from mantle to shallow depths within the crust.

Further studies are necessary in order to determine the structure and phase stability of nyerereite and related phases at H*P*/H*T* conditions.

## Implications

Our investigation helps to diagnose natural and synthetic alkaline and earth-alkaline carbonates by deciphering the structural characteristics of pure synthetic nyerereite with respect to natural samples. The accurate knowledge of the crystal structure of nyerereite allows us to speculate on its behavior at non ambient conditions, thus opening the possibility of a scenario where the

mineral has a wide stability field at pressure conditions higher than those applied during the synthesis experiments (100 MPa), consistent with H*P* experiments in the carbonate-silicate systems that revealed a number of Na-Ca carbonates resembling stoichiometries of $Na_2Ca(CO_3)_2$-nyerereite, $Na_2Ca_2(CO_3)_3$-shortite and $Na_2Ca_4(CO_3)_5$-burbankite (e.g., Kiseeva et al., 2013; Litasov et al., 2013; Thomson et al., 2016; Vennari et al., 2018; Rashchenko, 2020). Stabilization of Na-Ca carbonates at deep crust/mantle conditions, likely down to deep upper mantle and transition zone conditions, may have important implications for the solidus temperatures and formation of sodic dolomitic carbonatite melts and, in turn, the inner dynamic of the Earth. In fact, if at low pressure these melts are efficient transport agents of carbon from upper mantle to the crust due to their very low magmatic temperature and viscosity, at higher pressure we might expect changes in the carbonatitic minerals crystal structure also reflecting in changes in melt properties, e.g density and viscosity, that might influence the mobility of carbonate melts in the deep upper mantle / transition zone. Nyerereite, then, may be claimed as another carbonate mineral responsible for the storage of carbon in the deep Earth and its mobility from the mantle, or the deep crust, to the surface. This may have significant implications for the deep carbon cycle associated with carbonatites.

## Acknowledgements

The experiments were performed thanks to the financial program of the Department of Physics and Geology of the University of Perugia ("Fondo ricerca di Base 2018"; Principal Investigator AZ) and MIUR (project no. PRIN2017-2017LMNLAW "Connect4Carbon").

PNG, AVG, KK and AK were supported by the state assignment project of Sobolev Institute of Geology and Mineralogy SB RAS.

MC wishes to thank all the members of the Italian School of Paleoanthropology and of the Tanzania Human Origins Research (THOR) project (www.thorproject.it).

MRC acknowledges laboratory support from PRIN2017-2017J277S9.

## Reference

Abersteiner, A., Kamenetsky, V.S., Golovin, A.V., Kamenetsky, M., and Goemann, K. (2018a) Was crustal contamination involved in the formation of the serpentine-free Udachnaya-East kimberlite? New insights into parental melts, liquidus assemblage and effects of alteration. Journal of Petrology, 59, 1467-1492.

Abersteiner, A., Kamenetsky, V.S., Kamenetsky, M., Goemann, K., Ehrig, K., and Rodemann, T. (2018b) Significance of halogens (F, Cl) in kimberlite melts: Insights from mineralogy and melt inclusions in the Roger pipe (Ekati, Canada). Chemical Geology, 478, 148-163.

Abersteiner, A., Kamenetsky, V.S., Goemann, K., Giuliani, A., Howarth, G.H., Castillo-Oliver, M., Thompson, J., Kamenetsky, M., and Cherry, A. (2019) Composition and emplacement of the Benfontein Kimberlite Sill Complex (Kimberley, South Africa): Textural, petrographic and melt inclusion constraints. Lithos, 324-325, 297-314.

Abersteiner, A., Kamenetsky, V.S., Goemann, K., Kjarsgaard, B., Rodemann, T., Kamenetsky, M., and Ehrig, K. (2020) A genetic story of olivine crystallization in the Mark kimberlite (Canada) revealed by zoning and melt inclusions. Lithos, 358-359, 105405.

Alexandrov, E.V., Blatov, V.A., Kochetkov, A.V., and Proserpio, D.M. (2011) Underlying Nets in Three-Periodic Coordination Polymers: Topology, Taxonomy and Prediction from a Computer-Aided Analysis of the Cambridge Structural Database. CrystEngComm, 13, 3947−3958.

Alexandrov, E.V., Shevchenko, A.P., and Blatov, V.A. (2019) Topological Databases: Why Do We Need Them for Design of Coordination Polymers? Crystal Growth and Design, 19, 2604−2614.

Allison, C.M., Roggensack, K., and Clarke, A.B. (2021) Highly explosive basaltic eruptions driven by CO2 exsolution. Nature Communication, 12, 217.

Antao, S.M., and Hassan, I. (2009) The orthorhombic structure of $CaCO_3$, $SrCO_3$, $PbCO_3$ and $BaCO_3$: Linear structural trends. The Canadian Mineralogist, 47, 1245–1255.

Arzilli, F., Stabile, P., Fabbrizio, A., Landi, P., Scaillet, B., Paris, E., and Carroll, M.R. (2020) Crystallization Kinetics of Alkali Feldspar in Peralkaline Rhyolitic Melts: Implications for Pantelleria Volcano. Frontiers in Earth Science, 8, 177.

Attfield, J.P., and Férey, G. (1989) Structure determination of La2O2CO3-II and the unusual disordered phase La2O2.52(CO3)0.74Li0.52 using powder diffraction. Journal of Solid State Chemistry, 82, 132–138.

Baur, W.H. (1974) Acta Crystallographica, B30, 1195–1215.

Blatov, V.A. (2011) Crystal Structures of Inorganic Oxoacid Salts Perceived as Cation Arrays: A Periodic-Graph Approach. In: Vegas A. (eds) Inorganic 3D Structures. Structure and Bonding. Springer, Berlin, Heidelberg, 31–66.

Blatov, V.A., Shevchenko, A.P., and Proserpio, D.M. (2014) Applied Topological Analysis of Crystal Structures with the Program Package. Crystal Growth and Design, 14, 3576−3586.

Blatov, V.A. (2016) Method for Topological Analysis of Rod Packings. Structural Chemistry, 27, 1605−1611.

Bolotina, N.B., Gavryushkin, P.N., Korsakov, A.V., Rashchenko, S.V., Seryotkin, Y.V., Golovin, A.V., Moine, B.N., Zaitsev, A.N., and Litasov, K.D. (2017) Incommensurately modulated twin structure of nyerereite $Na_{1.64}K_{0.36}Ca(CO_3)_2$. Acta Crystallographica, B73, 276–284.

Borodina, U., Likhacheva, A., Golovin, A., Goryainov, S., Rashchenko, S., and Korsakov, A. (2018). Raman spectra of shortite $Na_2Ca_2(CO_3)_3$ compressed up to 8 GPa. High Pressure Research, 38, 293–302.

Brese, N.E., and O'Keeffe, M. (1991) Bond-valence parameters for solids. Acta Crystallographica B47, 192–197.

Bu, C., Rodriguez Lopez, G., Dukes, C.A., McFadden, L.A., Li, J-Y., and Ruesch, O. (2019) Stability of hydrated carbonates on Ceres. Icarus, 320, 136–149.

Campeny, M., Kamenetsky, V.S., Melgarejo, J.C., Mangas, J., Manuel, J., Alfonso, P., Kamenetsky, M.B., Bambi, A.C., and Gonçalves, A.O. (2015) Carbonatitic lavas in Catanda (Kwanza Sul, Angola): mineralogical and geochemical constraints on the parental melt. Lithos, 232, 1–11.

Carminati, E., Lustrino, M., and Doglioni, C. (2012) Geodynamic evolution of the central and western Mediterranean: Tectonics vs. igneous petrology constraints. Tectonophysics, 579, 173–192.

Cerantola, V., Bykova, E., Kupenko, I., Merlini, M., Ismailova, L., McCammon, C., Bykov, M., Chumakov, A.I., Petitgirard, S., Kantor, I., Svitlyk, V., Jacobs, J., Hanfland, M.,

Mezouar, M., Prescher, C., Rüffer, R., Prakapenka. V.B., and Dubrovinsky, L. (2017) Stability of iron-bearing carbonates in the deep Earth's interior. Nature Communication, 8, 15960.

Chen,W., Kamenetsky, V.S., and Simonetti, A. (2013) Evidence for the alkaline nature of parental carbonatite melts at Oka complex in Canada. Nature Communication, 4, 2687.

Comodi, P., Zucchini, A., Balić-Žunić, T., Hanfland, M., Collings, I. (2019) The High Pressure Behavior of Galenobismutite, $PbBi_2S_4$: A Synchrotron Single Crystal X-ray Diffraction Study. Crystals, 9, 210.

Cooper, A.F., Gittins, J., Tuttle, O.F. (1975) The system $Na_2CO_3$-$K_2CO_3$-$CaCO_3$ at 1 kilobar and its significance in carbonatite petrogenesis. American Journal of Science, 275, 534–560.

CrysAlisPRO, Oxford Diffraction /Agilent Technologies UK Ltd, Yarnton, England.

Dawson, J.B., Pinkerton, H., Norton G.E., and Pyle, D.M. (1990) Physico-chemical properties of alkali-carbonatite lavas, Tanzania. Geology 18, 260–263.

De Sanctis, M.C., Mitri, G., Castillo-Rogez, J., House, C.H., Marchi, S., Raymond, C.A., and Sekine, Y. (2020) Relict Ocean Worlds: Ceres. Space Science Reviews, 216, 60.

Di Matteo, V., Carroll, M. R., Behrens, H., Vetere, F., and Brooker, R. (2004). Water solubility in trachytic melts. Chemical Geology, 213, 187–196.

Dickens, B., Hyman, A., and Brown, W. (1971) Crystal structure of $Ca_2Na_2(CO_3)_3$ (shortite). Journal of Research of the National Bureau of Standards. Section A, Physics and Chemistry, 75, 129–140.

Donnay, G., Preston, H. (1971) Ewaldite, a new barium calcium carbonate. Tschermaks Mineralogische und Petrographische Mitteilungen, 15, 201–212.

Evans, H. T., and Milton, C. (1973) Crystallography of the heating products of gaylussite and pirssonite. American Mineralogist, 58, 1104.

Fabbrizio, A., Rouse, P. J., and Carroll, M. R. (2006). New experimental data on biotite+magnetite+sanidine saturated phonolitic melts and application to the estimation of magmatic water fugacity. American Mineralogist, 91, 1863–1870.

Fabbrizio, A., and Carroll, M. R. (2008). Experimental constraints on the differentiation process and pre-eruptive conditions in the magmatic system of Phlegrean Fields (Naples, Italy). Journal of Volcanology and Geothermal Research, 171, 88–102.

Fastelli, M., Zucchini, A., Comodi, P., Maturilli, A., Alemanno, G., Palomba, E., and Piergallini, R. (2021) NIR-MID Reflectance and Emissivity Study at Different Temperatures of Sodium Carbonate Minerals: Spectra Characterization and Implication for Remote Sensing Identification. Minerals, 11, 845.

Frankis. E.J., and McKie. D. (1973) Subsolidus Relations in the System $Na_2CO_3$-$CaCO_3$-$H_2O$. Nature Physical Science, 246, 124–126.

Frezzotti, M.L., Tecce, F., and Casagli, A. (2012) Raman spectroscopy for fluid inclusion analysis. Journal of Geochemical Exploration, 112, 1–20.

Frost, R.L., Bahfenne, S., and Graham J. (2009) Raman spectroscopic study of the magnesium-carbonate minerals – artiniteand dypingite. Journal of Raman Spectroscopy, 39, 855–860.

Gavryushkin, P.N., Bakakin, V.V., Bolotina, N.B., Shatskiy, A.F., Seryotkin, Y.V., and Litasov, K.D. (2014) Synthesis and crystal structure of new carbonate Ca3Na2 (CO3) 4 homeotypic with orthoborates M3Ln2 (BO3) 4 (M= Ca, Sr, and Ba). Crystal Growth & Design, 14, 4610-4616.

Gavryushkin, P.N., Thomas, V.G., Bolotina, N.D., Bakakin, V.V., Golovin, A.V., Seryotkin, Y.V., Fursenko, D.A., and Litasov, K.D. (2016) Hydrothermal Synthesis and Structure Solution of $Na_2Ca(CO_3)_2$: “Synthetic Analogue” of Mineral Nyerereite. Crystal Growth and Design, 16, 1893–1902.

Gavryushkin, P.N., Bekhtenova, A., Lobanov, S.S., Shatskiy, A., Likhacheva, A.Y., Sagatova, D., Sagatov, N., Rashchenko, S.V., Litasov, K.D., Sharygin, I.S., Goncharov, A.F., Prakapenka, V.B., and Higo, Y. (2019) High-pressure phase diagrams of $Na_2CO_3$ and $K_2CO_3$. Minerals, 9(10), 599.

Giuliani, A., Kamenetsky, V.S., Phillips, D., Kendrick, M.A., Wyatt, B.A., and Goemann, K. (2012) Nature of alkali-carbonate fluids in the sub-continental lithospheric mantle. Geology, 40, 967-970.

Giuliani, A., Soltys, A., Phillips, D., Kamenetsky, V.S., Maas, R., Woodhead, J.D., Drysdale, R.N., Goemann, K., and Griffin, W.L. (2017) The final stages of kimberlite petrogenesis: Petrography, mineral chemistry, melt inclusions and Sr-C-O isotope geochemistry of the Bultfontein kimberlite (Kimberley, South Africa). Chemical Geology, 455, 342-356.

Giuliani, A., Pearson, D.G., Soltys, A., Dalton, H., Phillips, D., Foley, S.F., Lim, E., Goemann, K., Griffin, W.L., and Mitchell, R.H. (2020) Kimberlite genesis from a common carbonate-rich primary melt modified by lithospheric mantle assimilation. Science Advances, 6, eaaz0424.

Golovin, A.V., Sharygin, V.V., Pokhilenko, N.P.,Mal'kovets, V.G., Kolesov, B.A., and Sobolev, N.V. (2003) Secondary melt inclusions in olivine from unaltered kimberlites of the Udachnaya-East pipe, Yakutia. Doklady Earth Sciences, 388, 93–96.

Golovin, A.V., Sharygin, V.V., and Pokhilenko, N.P. (2007) Melt inclusions in olivine phenocrysts in unaltered kimberlites from the Udachnaya-East pipe, Yakutia: some aspects of kimberlitemagma evolution during late crystallization stages. Petrology, 15, 168–183.

Golovin, A.V., Korsakov, A.V., and Zaitsev, A.N. (2015) In situ ambient and high-temperature Raman spectroscopic studies of nyerereite $(Na,K)_2Ca(CO_3)_2$: can hexagonal zemkorite be stable at earth-surface conditions? Journal of. Raman Spectroscopy, 46, 904–912.

Golovin, A.V., Sharygin, I.S., and Korsakov, A.V (2017a) Origin of alkaline carbonates in kimberlites of the Siberian craton: Evidence from melt inclusions in mantle olivine of the Udachnaya-East pipe. Chemical Geology, 455, 357-375.

Golovin, A.V., Korsakov, A.V., Gavryushkin, P.N., Zaitsev, A.N., Thomas, V.G., Moine, and B.N. (2017b) Raman spectra of nyerereite, gregoryite, and synthetic pure $Na_2Ca(CO_3)_2$: diversity and application for the study micro inclusions. Journal of Raman Spectroscopy, 48, 1559–1565.

Golovin, A.V., Sharygin, I.S., Kamenetsky, V.S., Korsakov, A.V., and Yaxley, G.M. (2018) Alkali-carbonate melts from the base of cratonic lithospheric mantle: Links to kimberlites. Chemical Geology, 483, 261-274.

Golovin, A.V., Sharygin, I.S., Korsakov, A.V., Kamenetsky, V.S., and Abersteiner, A. (2020) Can primitive kimberlite melts be alkali-carbonate liquids: Composition of the melt snapshots preserved in deepest mantle xenoliths. Journal of Raman Spectroscopy, 51(9), 1849-1867.

Golubkova, A., Merlini, M., and Schmidt, M.W. (2015) Crystal structure, high-pressure, and high-temperature behavior of carbonates in the $K_2Mg(CO_3)_2$–$Na_2Mg(CO_3)_2$ join. American Mineralogist, 100, 2458–2467.

Grassi, D., and Schmidt, M.W. (2011) The melting of carbonated pelites from 70 to 700 km depth. Journal of Petrology, 52, 765–789.

Guzmics, T., Mitchell, R.H., Szabo, C., Berkesi, M., Milke, R., and Abart, R. (2011) Carbonatite melt inclusions in coexisting magnetite, apatite and monticellite in Kerimasi calciocarbonatite, Tanzania:melt evolution and petrogenesis. Contribution to Mineralogy and Petrology, 161, 177–196.

588 Hammouda, T., Andrault, D., Koga, K., Katsura, T., and Martin, A.M. (2011) Ordering
589 in double carbonates and implications for processes at subduction zones. Contribution to
590 Mineralogy and Petrology, 161, 439–450.
591 Hübschle, C.B., Sheldrick, G.M., and Dittrich, B. (2011) ShelXle: a Qt graphical user
592 interface for SHELXL. Journal of Applied Crystallography, 44, 1281–1284.
593 Humphreys, E.R., Bailey, K., Hawkesworth, C.J., Wall, F., Najorka, J., and Rankin,
594 A.H. (2010) Aragonite in olivine from Calatrava, Spain—Evidence for mantle carbonatite
595 melts from >100 km depth. Geology, 38, 911–914.
596 Isakova, A.T., Panina, L.I., and Stoppa, F., (2017) Genesis of kalsilite melilitite at
597 Cupaello, Central Italy: evidence from melt inclusions. Petrology, 25, 433–447.
598 Isakova, A.T., Panina, L.I., and Stoppa, F. (2019) Formation conditions of leucite-
599 bearing lavas in the bolsena complex (Vulsini, Italy): research data on melt inclusions in
600 minerals. Russian Geology and Geophysics, 60(2), 119–132.
601 Jentzsch, P.V., Kampe, B., Ciobotă, V., Rösch, P., and Popp, J. (2013) Inorganic salts
602 in atmospheric particulate matter: Raman spectroscopy as an analytical tool. SAA, 115, 697–
603 708.
604 Johnson, D. R., and Robb, W. A. (1973) Gaylussite: Thermal properties by
605 simultaneous thermal analysis. American Mineralogist, 58, 778−784.
606 Káldos, R., Guzmics, T., Mitchell, R.H., Dawson, J.B., Milke, R., and Szabó, C. (2015)
607 A melt evolution model for Kerimasi volcano, Tanzania: evidence from carbonate melt
608 inclusions in jacupirangite. Lithos, 238, 101–119.
609 Kamenetsky, V.S., Kamenetsky, M.B., Weiss, Y., Navon, O., Nielsen, T.F.D., and
610 Mernagh, T.P. (2009) How unique is the Udachnaya-East kimberlite? Comparison with
611 kimberlites from the Slave Craton (Canada) and SW Greenland. Lithos, 112, 334-346.

612 Kamenetsky, V.S., Kamenetsky, M.B., Golovin, A.V., Sharygin, V.V., and Maas, R.
613 (2012) Ultrafresh salty kimberlite of the Udachnaya–East pipe (Yakutia, Russia): a petrological
614 oddity or fortuitous discovery? Lithos, 152, 173–186.

615 Kamenetsky, V.S., Grütter, H., Kamenetsky, M.B., and Gömann, K. (2013) Parental
616 carbonatitic melt of the Koala kimberlite (Canada): constraints from melt inclusions in olivine
617 and Cr-spinel, and groundmass carbonate. Chemical Geologt, 353, 96-111.

618 Kaminsky, F., Wirth, R., Matsyuk, S., Schreiber, A., and Thomas, R. (2009) Nyerereite
619 and nahcolite inclusions in diamond: evidence for lower-mantle carbonatitic magmas.
620 Mineralogical Magazine, 73, 797–816.

621 Keller, J., and Zaitsev, A.N. (2012) Geochemistry and petrogenetic significance of
622 natrocarbonatites at Oldoinyo Lengai, Tanzania: Composition of lavas from 1988 to 2007.
623 Lithos, 148, 45–53.

624 Kiseeva, E.S., Litasov, K.D., Yaxley, G.M., Ohtani, E., and Kamenetsky, V.S. (2013)
625 Melting and phase relations of carbonated eclogite at 9–21 GPa and the petrogenesis of
626 alkalirich melts in the deep mantle. Journal of Petrology, 54, 1555–1583.

627 Kogarko, L., Plant, D., Henderson, C., and Kjarsgaard, B. (1991) Na-rich carbonate
628 inclusions in perovskite and calzirtite fromthe Guli intrusive Ca-carbonatite, polar Siberia.
629 Contribution to Mineralogy and Petrology, 109, 124–129.

630 Kogarko, L.N., and Veselovskiy, R.V. (2019) Geodynamic origin of carbonatites from
631 the absolute paleotectonic reconstructions. Journal of Geodynamics, 125, 13–21.

632 Krafft, M., and Keller, J. (1989) Temperature measurements in carbonatite lava lakes
633 and flows from Oldoinyo Lengai, Tanzania. Science, 245(4914), 168–170.

634 Kutlu, I., and Meyer G. (1999) Basische Carbonate des Dysprosiums: $Dy_2O_2(CO_3)$ und
635 $Dy(OH)(CO_3)$. Zeitschrift für anorganische und allgemeine Chemie, 625, 402–406.

Lafuente, B., Downs, R.T., Yang, H., and Stone, N. (2016) The power of databases: the RRUFF project. Pp. 1-29 in: Highlights in Mineralogical Crystallography (T. Armbruster and R.M. Danisi editors). Walter de Gruyter GmbH, Berlin, Germany.

Litasov, K.D., Shatskiy, A., Ohtani, E., and Yaxley, G.M. (2013) Solidus of alkaline carbonatite in the deep mantle. Geology, 41, 79–82.

Liu, Y., Shen, Y., Zhao, S., and Luo, J. (2020) Structure-property relationship in nonlinear optical materials with π-conjugated $CO_3$ triangles. Coordination Chemistry Reviews, 407, 213152.

Lustrino, M., Luciani, N., and Stagno, V. (2019) Fuzzy petrology in the origin of carbonatitic/pseudocarbonatitic Ca-rich ultrabasic magma at Polino (central Italy). Scientific Reports, 9, 9212.

Marchand, R., Piffard, Y., and Tournoux, M. (1975) Structure cristalline de $Tl_2CO_3$. Canadian Journal of Chemistry, 53, 2454–2458.

Mattsson, H.B., Balashova, A., Almqvist, B.S.G., Bosshard-Stadlin, S.A., and Weidendorfer, D. (2018) Magnetic mineralogy and rock magnetic properties of silicate and carbonatite rocks from Oldoinyo Lengai volcano (Tanzania). Journal of African Earth Sciences, 142, 193–206.

McCord, T.B., Hansen, G.B., Fanale, F.P., Carlson, R.W., Matson, D.L., Johnson, T.V., Smythe, W.D., Crowley, J.K., Martin, P.D., Ocampo, A., Hibbitts, C.A., and Granahan, J.C. (1998) the NIMS Team. Salts on Europa's Surface Detected by Galileo's Near Infrared Mapping Spectrometer. Science, 280, 1242–1245.

McKie, D., and Frankis, E.J. (1977) Nyerereite: A new volcanic carbonate mineral from Oldoinyo Lengai, Tanzania. Zeitschrift fur Kristallographie, 145, 73–95.

Merlini, M., Crichton, W.A., Hanfland, M., Gemmi, M., Müller, E., Kupenko, I., and Dubrovinsky, L. (2012) Structures of dolomite at ultrahigh pressure and their influence on the deep carbon cycle. PNAS, 109, 13509–13514.

Merlini, M., Sapelli, F., Fumagalli, P., Gatta, G.D., Lotti, P., Tumiati, S., Aabdellatief, M., Lausi, A., Plaisier, J., Hanfland, M., Crichton, W., Chantel, J., Guignard, J., Meneghini, C., Pavese, A., and Poli, S. (2016) High-temperature and high-pressure behavior of carbonates in the ternary diagram $CaCO_3$-$MgCO_3$-$FeCO_3$. American Mineralogist, 101(6), 1423–1430.

Mitchell, R.H., and Kamenetsky, V.S. (2012) Trace element geochemistry of nyerereite and gregoryite phenocrysts fromnatrocarbonatite lava, Oldoinyo Lengai, Tanzania: implications for magma mixing. Lithos, 152, 56–65.

Momma, K., and Izumi, F. (2011). VESTA 3 for three-dimensional visualization of crystal, volumetric and morphology data. Journal of Applied Crystallography, 44, 1272-1276.

Nagai, T., Ito, T., Hattori, T., and Yamanaka, T. (2000) Compression mechanism and amorphization of portlandite, Ca(OH)2: structural refinement under pressure. Physics and Chemistry of Minerals, 27, 462–466.

Nixon, D.E., Parry, G.S., and Ubbelohde, A.R. (1966) Order-disorder transformations in graphite nitrates. Proceedings of the Royal Society of London, Series A: Mathematical and Physical Sciences, 291, 324–339.

O'Keeffe, M., Peskov, M.A., Ramsden, S.J., and Yaghi, O.M. (2008) The Reticular Chemistry Structure Resource (RCSR) database of, and symbols for, crystal nets. Accounts of Chemical Research, 41, 1782–1789.

Oppenheimer, C. (1998) Satellite observation of active carbonatite volcanism at Ol Doinyo Lengai, Tanzania. International Journal of Remote Sensing, 19(1), 55–64.

683 Panina, L.I., Stoppa, F., and Usol'tseva, L.M. (2003) Genesis of melilitite rocks of Pian
684 di Celle volcano, umbrian kamafugite province, Italy: evidence from melt inclusions in
685 minerals. Petrology, 11(4), 365–382.

686 Paone, A. (2013) A Review of Carbonatite Occurrences in Italy and Evaluation of
687 Origins. Open Journal of Geology, 3, 66–82.

688 Parthasarathy, G., Chetty, T.R.K., and Haggerty, S.E. (2002) Thermal stability and
689 spectroscopic studies of zemkorite: a carbonate from the Venkatampalle kimberlite of southern
690 India. American Mineralogist, 87 (10), 1384–1389.

691 Peccerillo, A. (2017) The Intra-Apennine Province. In: Cenozoic Volcanism in the
692 Tyrrhenian Sea Region. (Springer, Cham) pp. 61–79.

693 Peterson, T.D. (1990) Petrology and genesis of natrocarbonatite. Contribution to
694 Mineralogy and Petrology, 105, 143–155.

695 Pertlik, F. (1981) Structural investigations of synthetic fairchildite, $K_2Ca(CO_3)_2$.
696 Zeitschrift für Kristallographie, 157, 199–205.

697 Podborodnikov, I.V., Shatskiy, A., Arefiev, A.V., Rashchenko, S.V., Chanyshev, A.D.,
698 and Litasov, K.D. (2018) The system $Na_2CO_3$–$CaCO_3$ at 3 GPa. Physics and Chemistry of
699 Minerals, 45, 773–787.

700 Postberg, F., Schmidt, J., Hillier, J., Kempf, S., and Srama, R. (2011) A salt-water
701 reservoir as the source of a compositionally stratified plume on Enceladus. Nature, 474, 620–
702 622.

703 Prewitt, C.T., and Downs, R.T. (1998) High-pressure crystal chemistry, in Ultrahigh-
704 Pressure Mineralogy: Physics and Chemistry of Earth's Deep Interior, edited by R. J. Hemley,
705 Rev. Mineral., vol. 37, pp. 283–317, Mineral. Soc. of Am., Washington, D.C..

Rashchenko, S.V., Shatskiy, A.F., Arefiev, A.V., Seryotkin, Y.V., and Litasova, K.D. (2018) "$Na_4Ca(CO_3)_3$: a novel carbonate analog of borate optical materials." CrystEngComm, 35, 5228–5232.

Rashchenko, S.V., Shatskiy, A.F., and Litasov, K.D. (2020) High-Pressure Na-Ca Carbonates in the Deep Carbon Cycle. In Carbon in Earth's Interior (eds C.E. Manning, J.-F. Lin and W.L. Mao).

Rosatelli, G., Wall, F., Stoppa, F. (2007) Calcio-carbonatite melts and metasomatism in the mantle beneath Mt. Vulture (Southern Italy). Lithos, 99, 229–248.

Sharygin, I.S., Litasov, K.D., Shatskiy, A., Safonov, O.G., Golovin, A.G., Ohtani, E., and Pokhilenko, N.P. (2017) Experimental constraints on orthopyroxene dissolution in alkali-carbonate melts in the lithospheric mantle: Implications for kimberlite melt composition and magma ascent. Chemical Geology, 455, 44–56.

Shatskiy, A., Gavryushkin, P.N., Sharygin, I.S., Litasov, K.D., Kupriyanov, I.N., Higo, Y., Borzdov, Y.M., Funakoshi, K., Palyanov, Y.N., and Ohtani, E. (2013) Melting and subsolidus phase relations in the system $Na_2CO_3$-$MgCO_3$±$H_2O$ at 6 GPa and the stability of $Na_2Mg(CO_3)_2$ in the upper mantle. American Mineralogist, 98, 2172–2182.

Shatskiy, A., Gavryushkin, P.N., Litasov, K.D., Koroleva, O.N., Kupriyanov, I.N., Borzdov, Y.M., Sharygin, I.S., Funakoshi, K., Palyanov, Y.N., and Ijiohtani, E. (2015) Na-Ca carbonates synthesized under upper-mantle conditions: Raman spectroscopic and X-ray diffraction studies. European Journal of Mineralogy, 27, 175 – 184.

Smith, J. W., Johnson, D. R., and Robb, W. A. (1971) Thermal synthesis of sodium calcium carbonate − a potential thermal analysis standard. Thermochimica Acta, 2, 305−312.

Sokolov, S., Yarmishko, S., and Chistyakova, N. (2006) Inclusions in chrysolite from the Kovdor Massif: Genetic and gemological significance. Geochemistry International, 44, 581–590.

Song, Y., Luo, M., Zhao, D., Peng, G., Lina, C., and Ye, N. (2017) Explorations of new UV nonlinear optical materials in the $Na_2CO_3$–$CaCO_3$ system. Journal of Material Chemistry C, 5, 8758.

Stabile, P., Radica, F., Bello, M., Behrens, H., Carroll, M. R., Paris, E., et al. (2018). $H_2O$ solubility in pantelleritic melts: pressure and alkali effects. J. Min. Geochem. 195, 1–9.

Stabile P., Appiah E., Bello M., Giuli G., Paris E., and Carroll M.R. (2020) New IR spectroscopic data for determination of water abundances in hydrous pantelleritic glasses. American Mineralogist, 105, 1060–1068.

Stoppa, F., Jones, A.P., and Sharygin, V.V. (2009) Nyerereite from carbonatite rocks at Vulture volcano: implications for mantle metasomatism and petrogenesis of alkali carbonate melts Research Article. Central European Journal of Geosciences, 1, 131–151.

Stoppa, F., and Lavecchia, G. (1992) Late Pleistocene ultra-alkaline magmatic activity in the Umbria-Latium region (Italy): An overview. Journal of Volcanology and Geothermal Research, 52, 277–293.

Stoppa, F., Schiazza, M., Rosatelli, G., Castorina, F., Sharygin, V.V., Ambrosio, F.A., and Vicentini, N. (2019) Italian Carbonatite System: from Mantle to Ore-deposit 2019. Ore Geology Reviews, 114, 103041.

Thomson, A.R., Walter, M.J., Kohn, S.C., and Brooker, R.A. (2016) Slab melting as a barrier to deep carbon subduction. Nature, 529, 76–79.

Veksler, I., Nielsen, T., and Sokolov, S. (1998). Mineralogy of crystallized melt inclusions from Gardiner and Kovdor ultramafic alkaline complexes: implications for carbonatite genesis. Journal of Petrology, 39, 2015–2031.

Vennari, C.E., Beavers, C.M., and Williams, Q. (2018) High-Pressure/Temperature Behavior of the Alkali/Calcium Carbonate Shortite ($Na_2Ca_2(CO_3)_3$): Implications for Carbon Sequestration in Earth's Transition Zone. JGR, 123, 6574–6591.

Vilaplana, R., Parra, S.G., Jorge-Montero, A., Rodríguez-Hernández, P., Munoz, A., Errandonea, D., Segura, A., and Manjón, F.J. (2018) Experimental and Theoretical Studies on α-In2Se3 at High Pressure. Inorganic Chemistry, 57, 8241–8252.

Wang, J., and Becker, U. (2009) Structure and carbonate orientation of vaterite ($CaCO_3$). American Mineralogist, 94, 380–386.

Zaitsev, A.N., and Chakhmouradian, A.R., (2002) Calcite–amphibole–clinopyroxene rock from the Afrikanda complex, Kola Peninsula, Russia: mineralogy and a possible link to carbonatites. II. Oxysalt minerals. The Canadian Mineralogist, 40, 103–120.

Zaitsev, A.N., and Keller, J. (2006) Mineralogical and chemical transformation of Oldoinyo Lengai natrocarbonatites, Tanzania. Lithos, 1 – 4, 191 – 207.

Zaitsev, A.N., Keller, J., Spratt, J., Perova, E.N., and Kearsley, A. (2008) Nyerereite-pirssonite-calcite-shortite relationships in altered natrocarbonatites, Oldoinyo Lengai, Tanzania. The Canadian Mineralogist, 46, 843–860.

Zaitsev, A.N., Keller, J., Spratt, J., Jeffries, T.E., and Sharigin, V.V. (2009) Chemical composition of nyerereite and gregoryite from natrocarbonatites of Oldoinyo Lengai volcano, Tanzania. Geology of Ore Deposits, 51(7), 608–616.

Zaitsev, A.N., Wenzel, T., Vennemann, T., and Markl, G., (2013) Tinderet volcano, Kenya: an altered natrocarbonatite locality?. Mineralogical Magazine, 77, 213–226.

Zaitsev, A.N. (2010) Nyerereite from calcite carbonatite at Kerimasi volcano, northern Tanzania. Geology of Ore Deposits, 52, 630–640.

Zucchini, A., Comodi, P., Nazzareni, S., and Hanfland, M. (2014) The effect of cation ordering and temperature on the high-pressure behavior of dolomite. Physics and Chemistry of Minerals, 41, 783–793.

779 Zucchini, A., Prencipe, M., Belmonte, D., Comodi, P. (2017) Ab initio study of the
780 dolomite to dolomite-II high-pressure phase transition. European Journal of Mineralogy, 29(2),
781 227–238.

782

## Figures captions

**FIGURE 1.** Reflected light microscope images of NMAG (a, b) and NHD15 (c, d). Magnifications are 4x (a, c) and 20x (b, d).

**FIGURE 2.** Backscattered electron images showing products of experiments NMAG (a), NHD15 (b).

**FIGURE 3.** Comparison of the position of strong Raman lines for three separate grains of different orientations, obtained in the NHD15 experiments (top) as compared with spectra from Golovin et al. (2017) (bottom).

**FIGURE 4.** Raman spectra of the mixed areas, divided in four regions where the most intense Raman signals due to $CO_3^{2-}$ vibrations are present (after Golovin et al., 2017b; Vennari et al., 2018): (a) spectral region where vibrations are due to the interaction between carbonate groups and Na-Ca sublattices, (b) spectral region that shown the $\nu_4(CO_3)^{2-}$ (in-plane bending) vibrations, (c) spectral region where the $\nu_1(CO_3)^{2-}$ (symmetric stretching) vibrations lie, and (d) water spectral region. Colors are attributed according to the legend shown in (a). Solid line spectra are the collected Raman spectra in the present work. The dashed dark red spectra are Raman data collected in three nyerereite crystals from Golovin et al. (2017b). Vertical lines represent the position of the Raman signals in reference data as follows: dotted orange is γ-$Na_2CO_3$ (Shatskiy et al., 2015) and dashed red is thermonatrite (Jentzsch et al., 2013; Frezzotti et al., 2012). The arrow in a) shows the position of the unassigned signal.

**FIGURE 5.** $CaCO_3$ (top left) and $Na_2CO_3$ layers (top right) constituting nyerereite crystal structure and their superimposition in nyerereite crystal structure (bottom). Ca, Na, $C(1)O_3$ and $C(2)O_3$ atoms are colored in blue, yellow, dark brown and light brown, respectively.

**FIGURE 6.** Representation of a portion of the nyerereite unit cell content where selected atomic sites are shown for the Na1 and Na2 in yellow, Ca in blue, C1 in dark brown and C2 in light

808 brown. A schematic representation of the bond length for the O4, O5 and O6 atoms bonding
809 C2 is illustrated being the sawtooth and the dashed lines the highest the lowest bond-valences,
810 respectively.

811 **FIGURE 7.** Crystal structure of (a) nyerereite and (b) aragonite in the (*ab*) plane. Aragonite is
812 shown in the 2 × 1 × 2 supercell to highlight the similarities with nyerereite. Colors are as
813 follows: yellow is Na; blue is Ca; red is O; dark and light brown are C1 (in nyerereite and
814 aragonite) and C2 (in nyerereite), respectively. Figures were made by VESTA software
815 (Momma and Izumi, 2011).

816

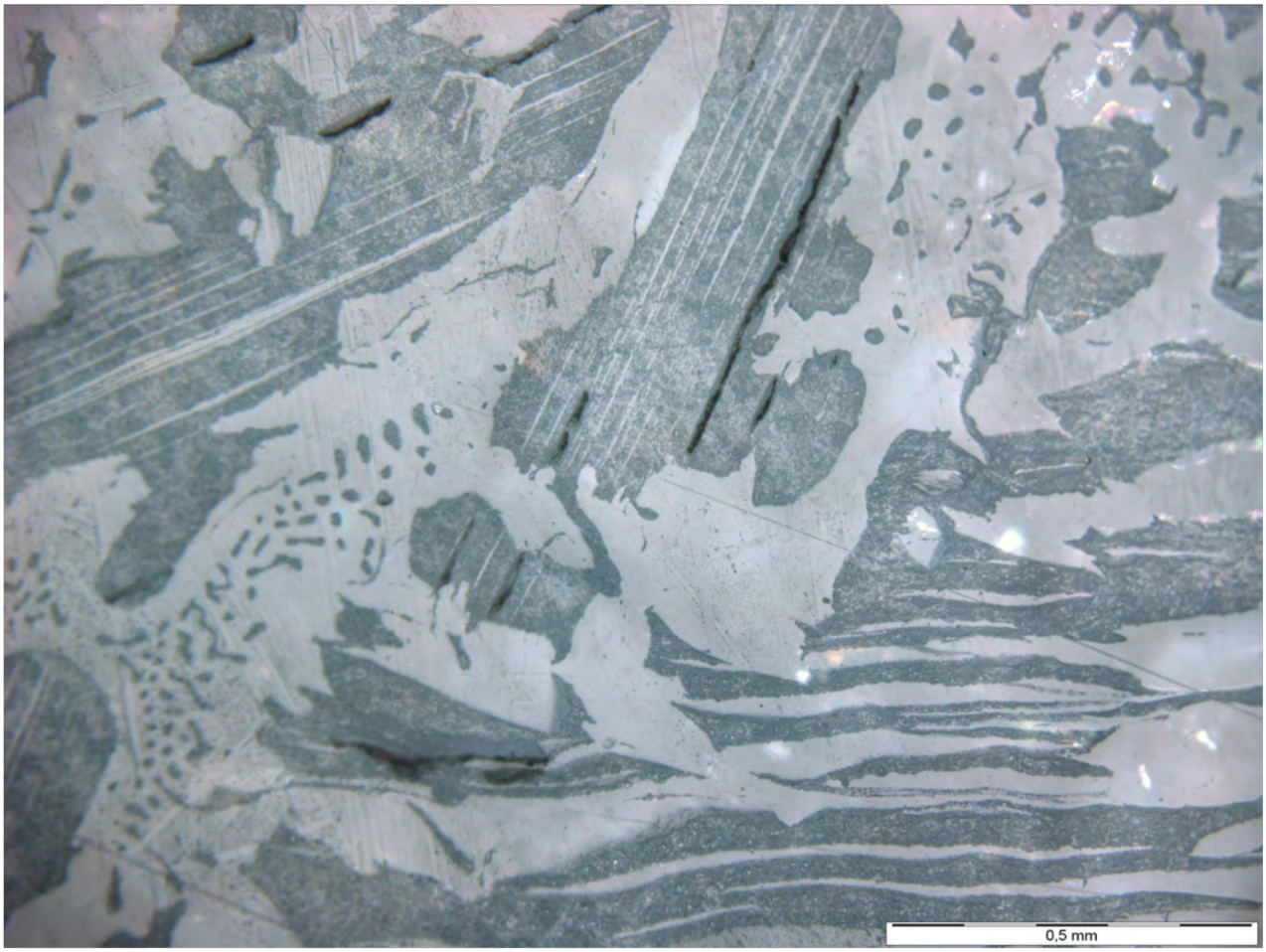


Figure 1a

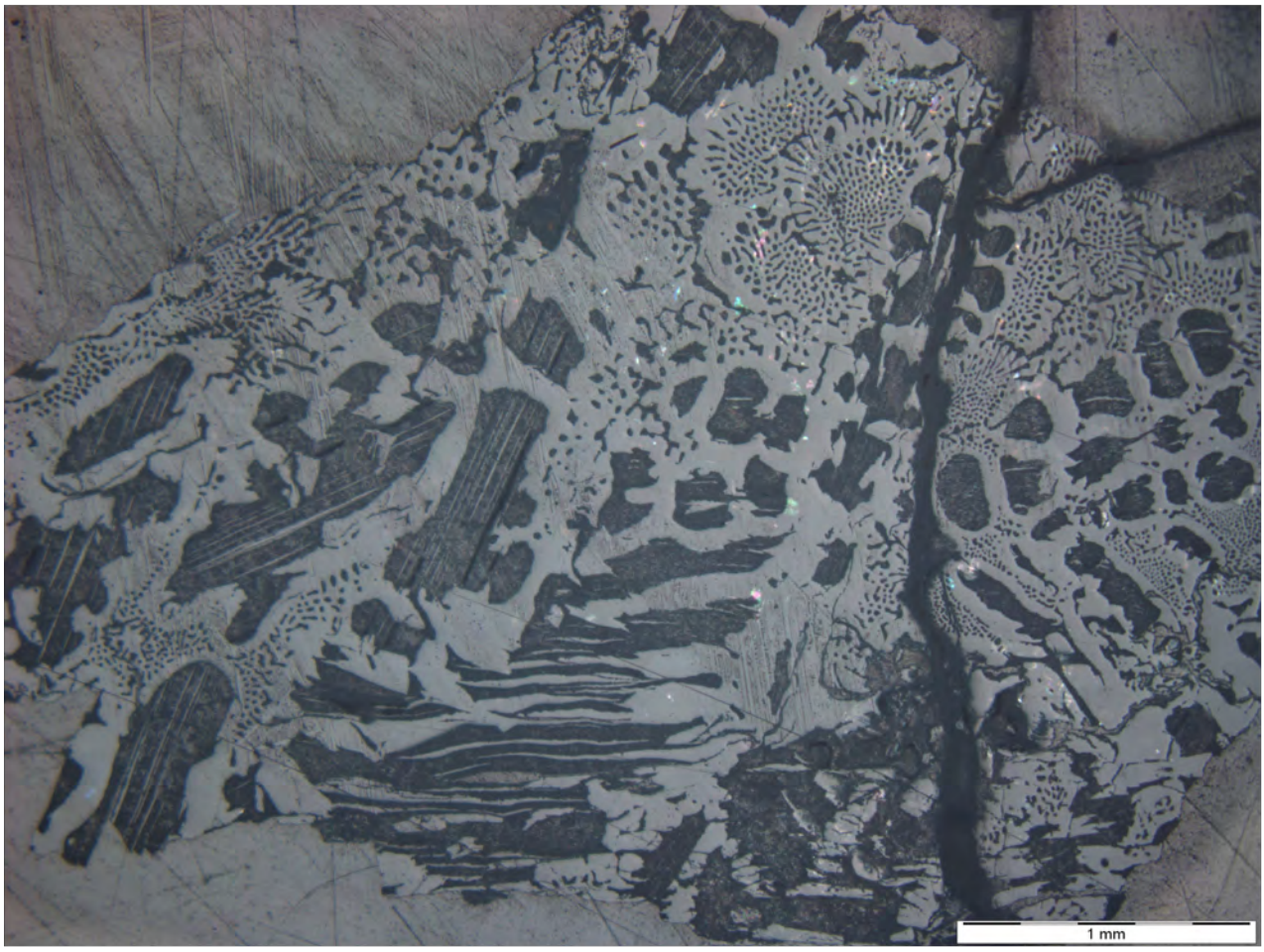


Figure 1b

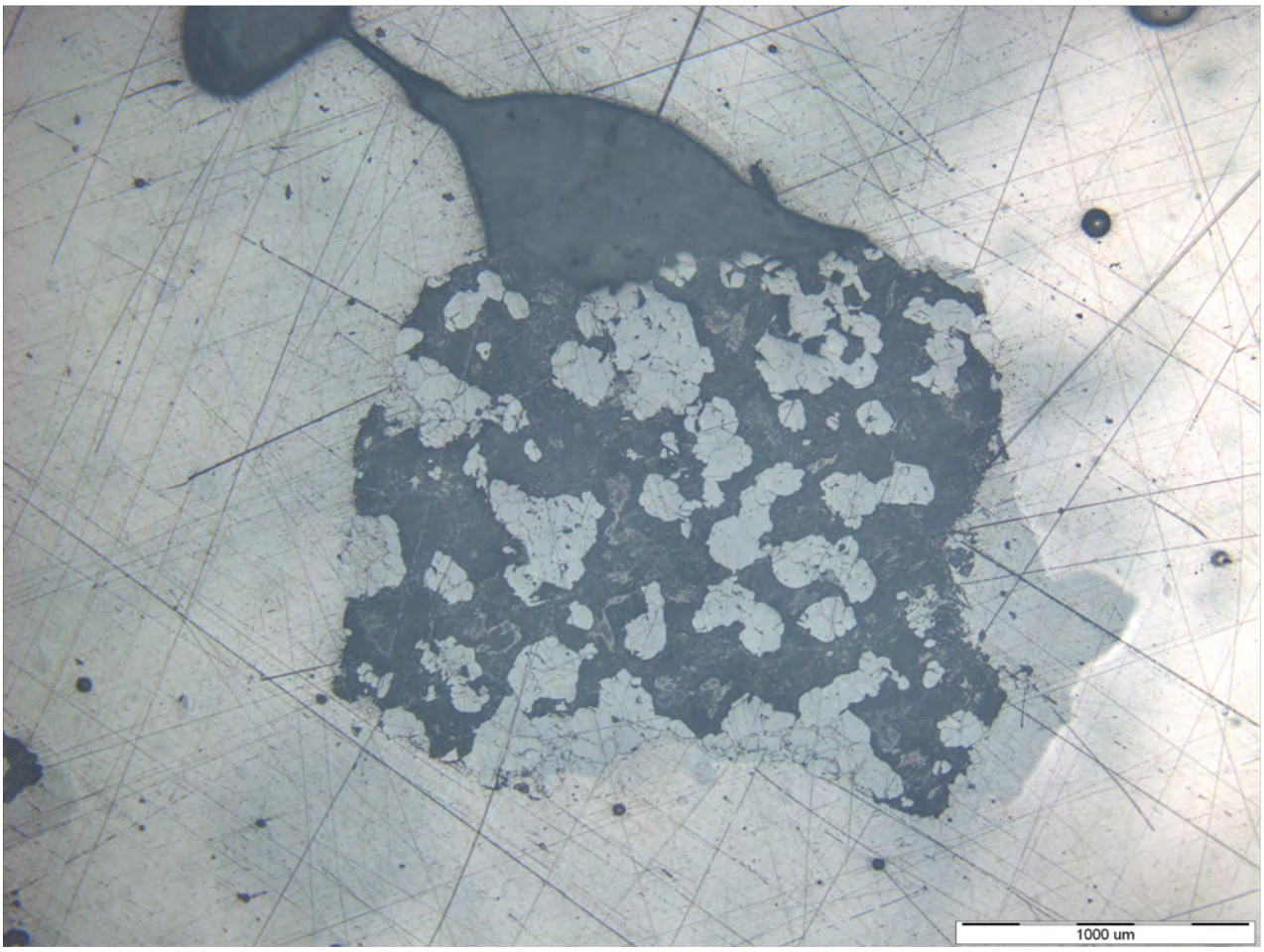


Figure 1c

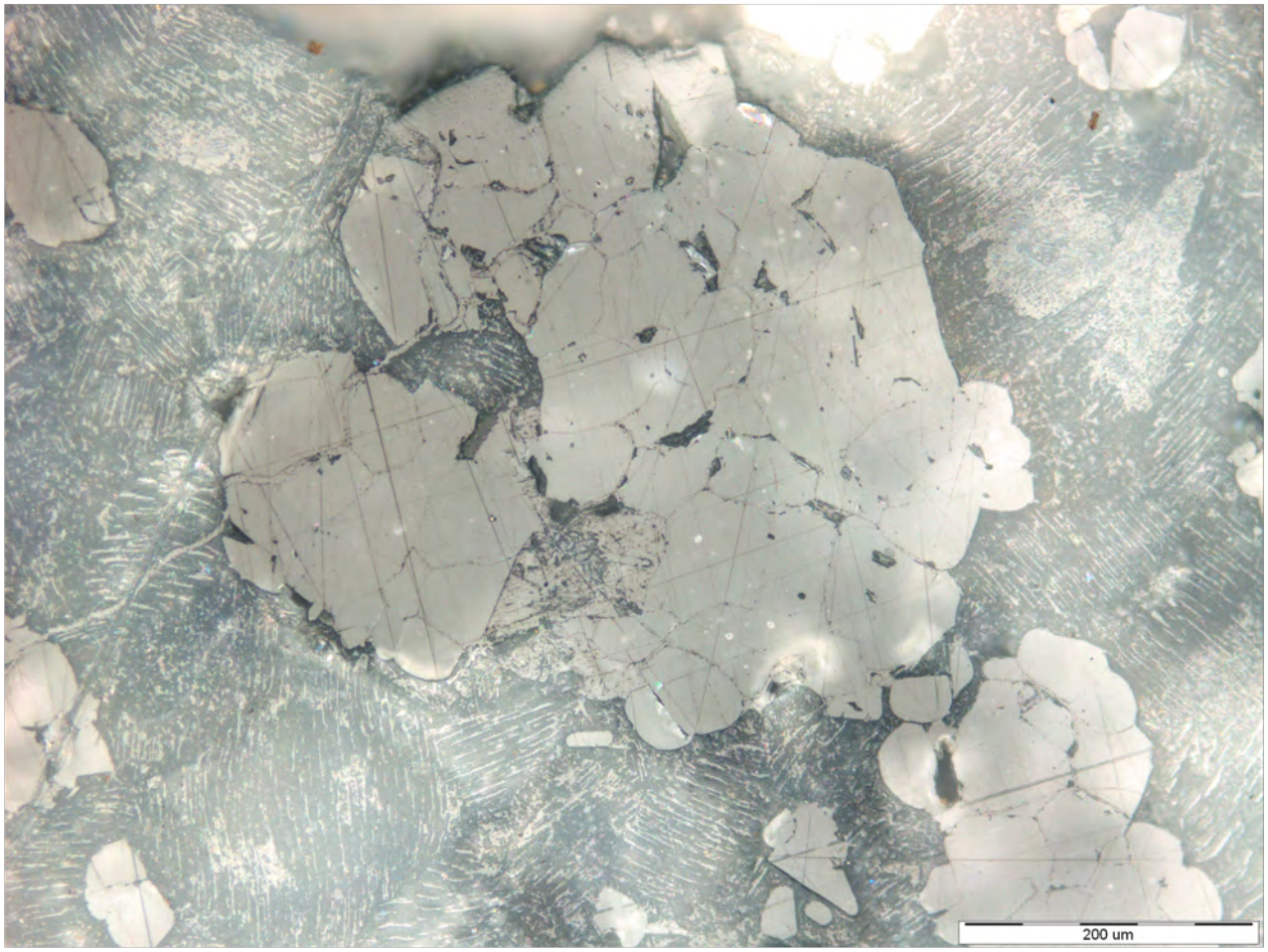


Figure 1d

This is the peer-reviewed, final accepted version for American Mineralogist, published by the Mineralogical Society of America.
The published version is subject to change. Cite as Authors (Year) Title. American Mineralogist, in press.
DOI: https://doi.org/10.2138/am-2022-8106. http://www.minsocam.org/

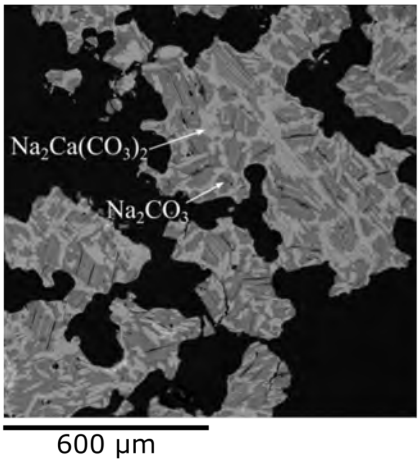


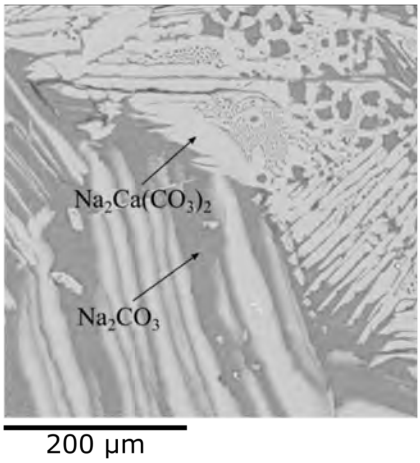


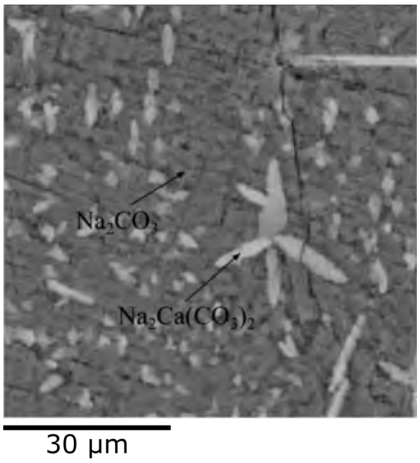


Figure 2a

This is the peer-reviewed, final accepted version for American Mineralogist, published by the Mineralogical Society of America.
The published version is subject to change. Cite as Authors (Year) Title. American Mineralogist, in press.
DOI: https://doi.org/10.2138/am-2022-8106. http://www.minsocam.org/

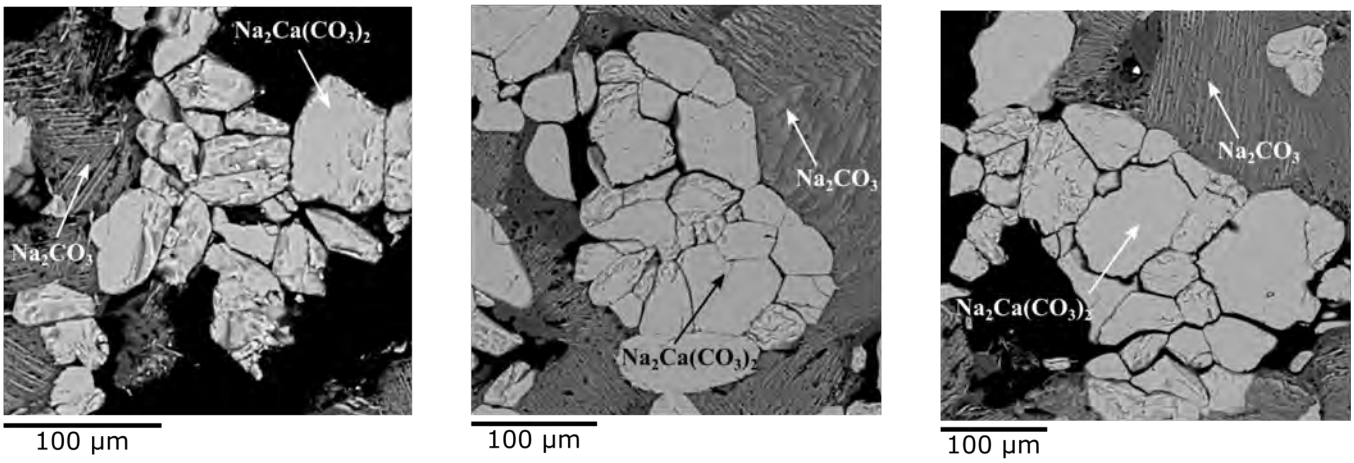


Figure 2b

This is the peer-reviewed, final accepted version for American Mineralogist, published by the Mineralogical Society of America.
The published version is subject to change. Cite as Authors (Year) Title. American Mineralogist, in press.
DOI: https://doi.org/10.2138/am-2022-8106. http://www.minsocam.org/

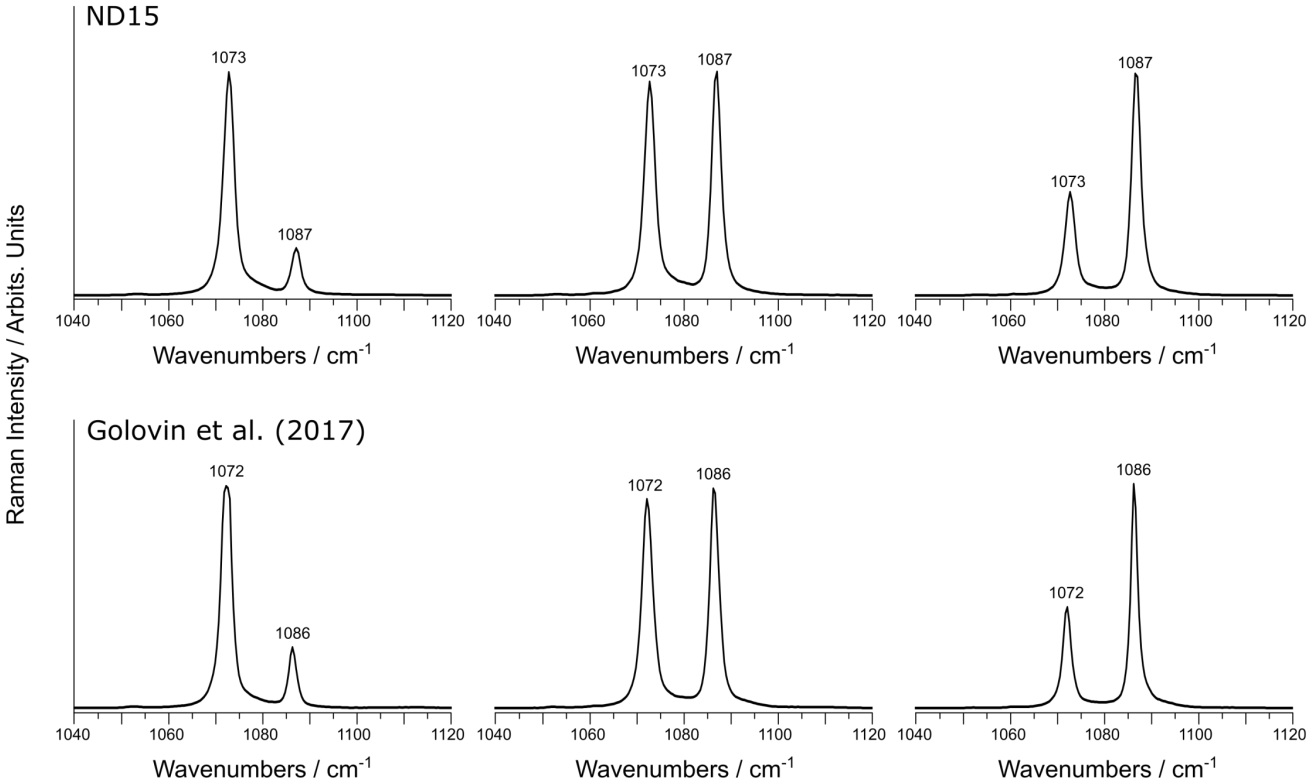


Figure 3

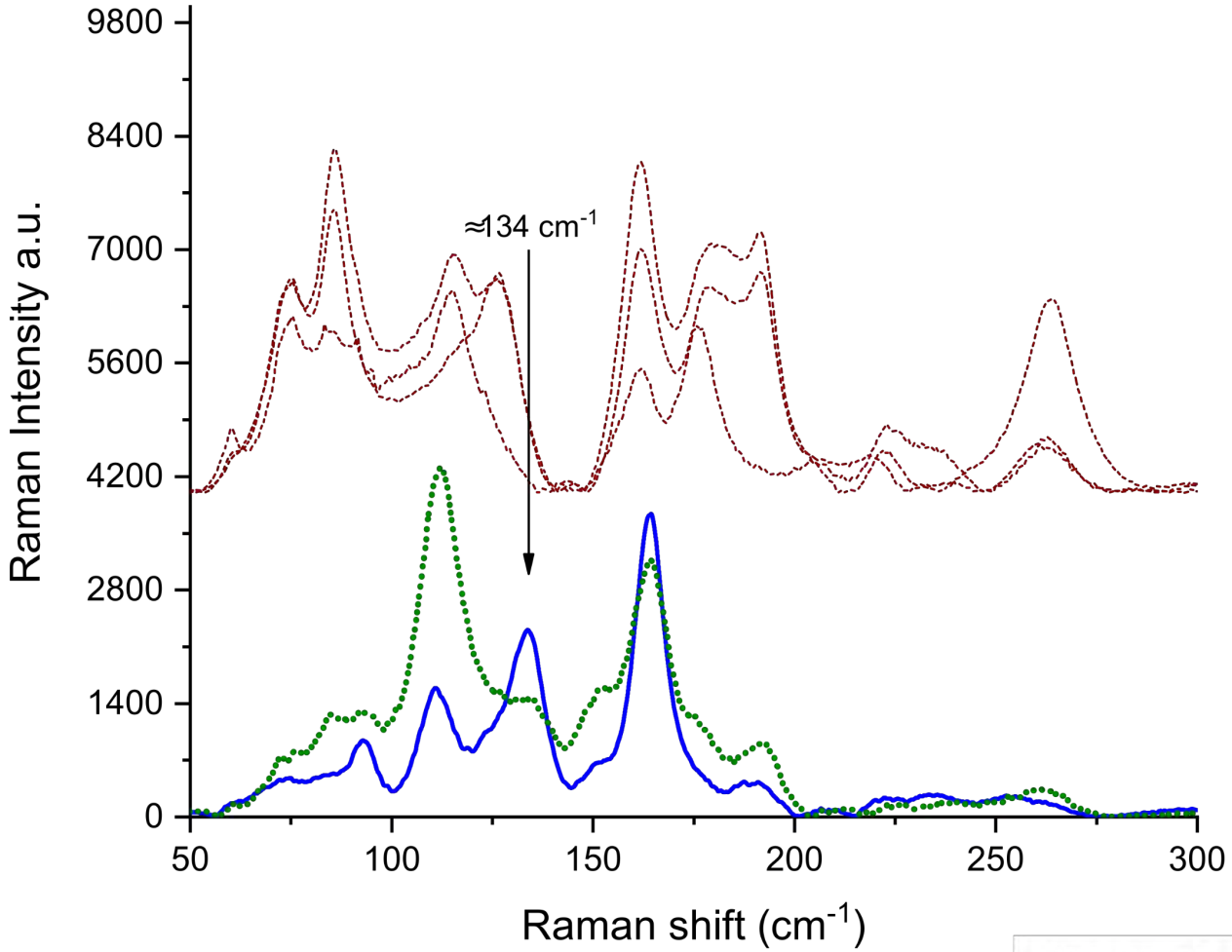


Figure 4a

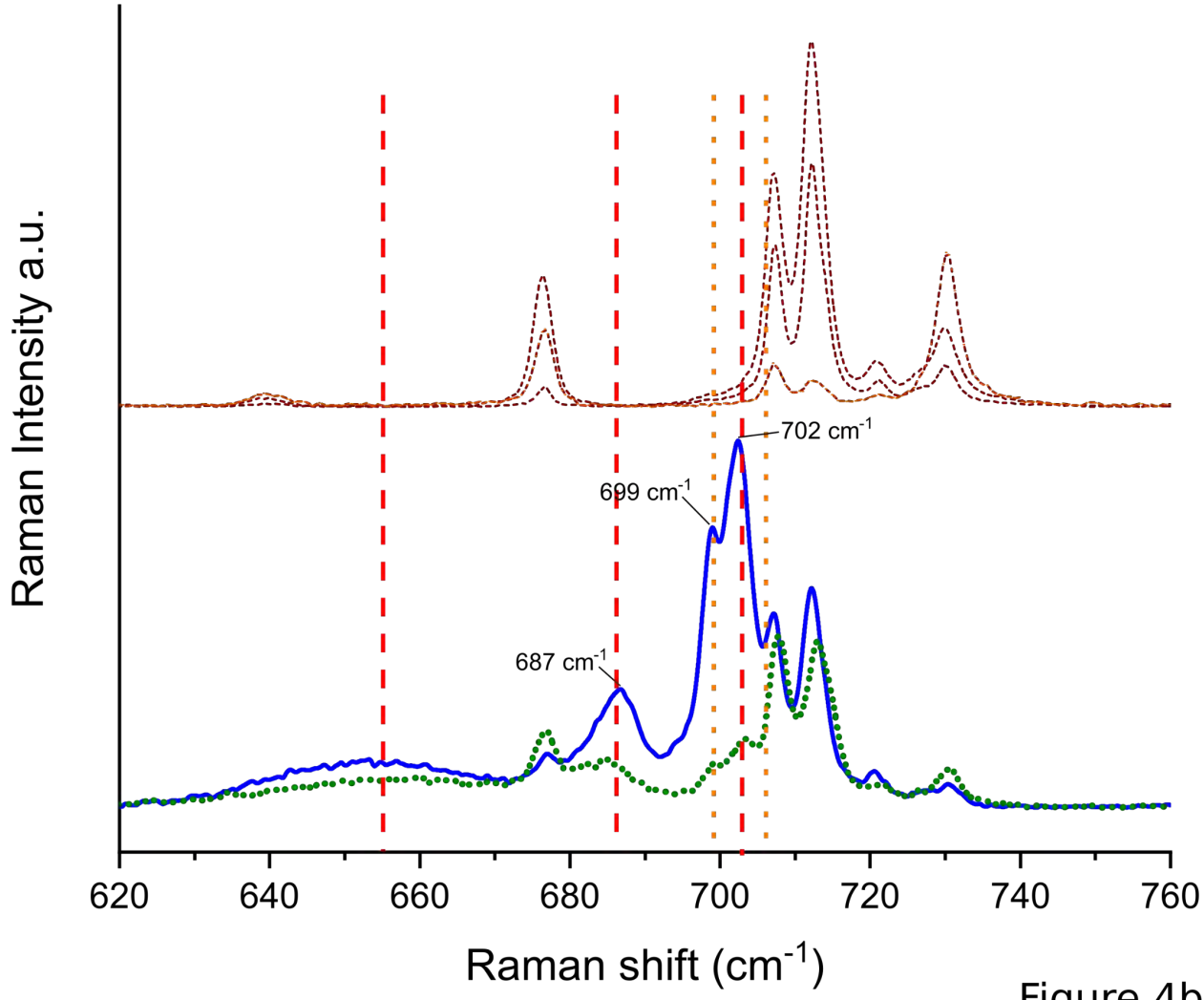


Figure 4b

This is the peer-reviewed, final accepted version for American Mineralogist, published by the Mineralogical Society of America.
The published version is subject to change. Cite as Authors (Year) Title. American Mineralogist, in press.
DOI: https://doi.org/10.2138/am-2022-8106. http://www.minsocam.org/

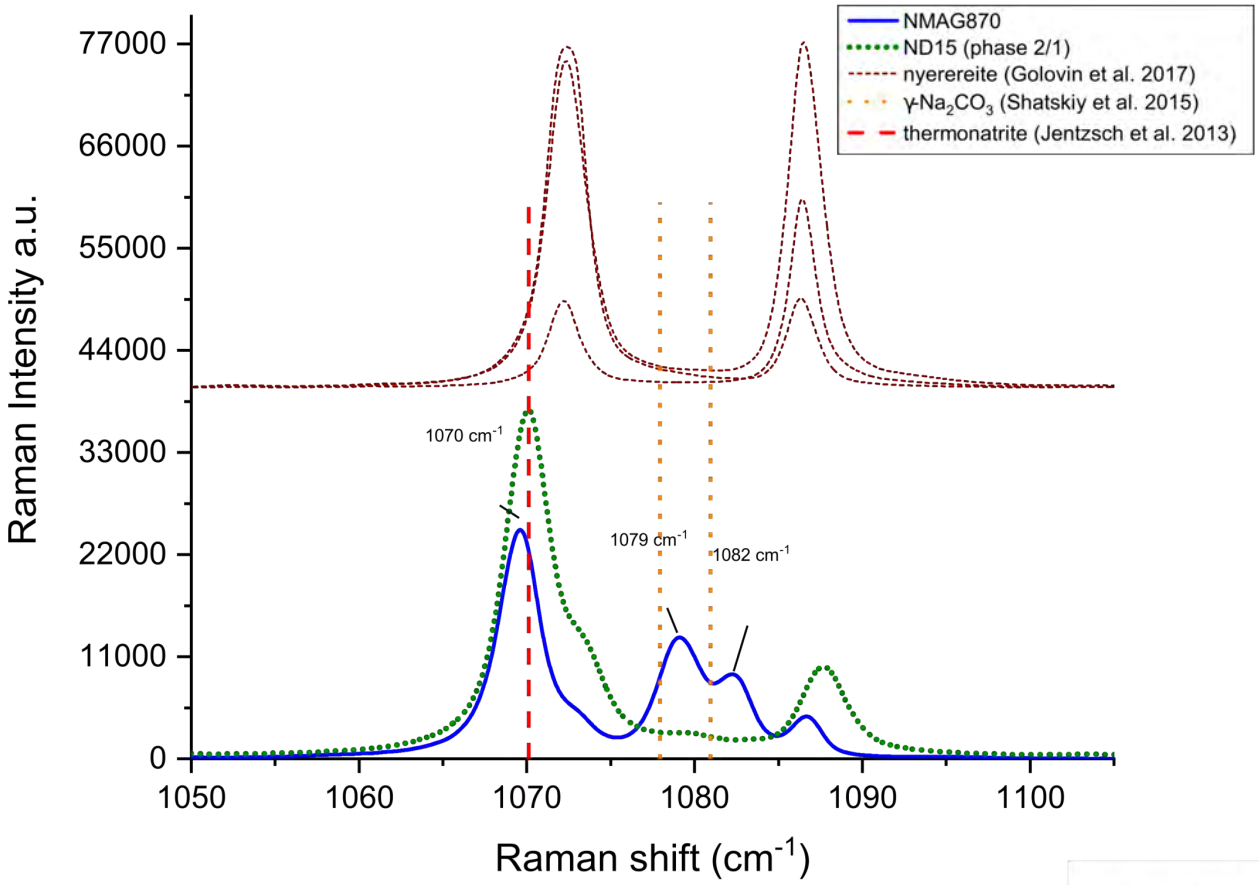


Figure 4c

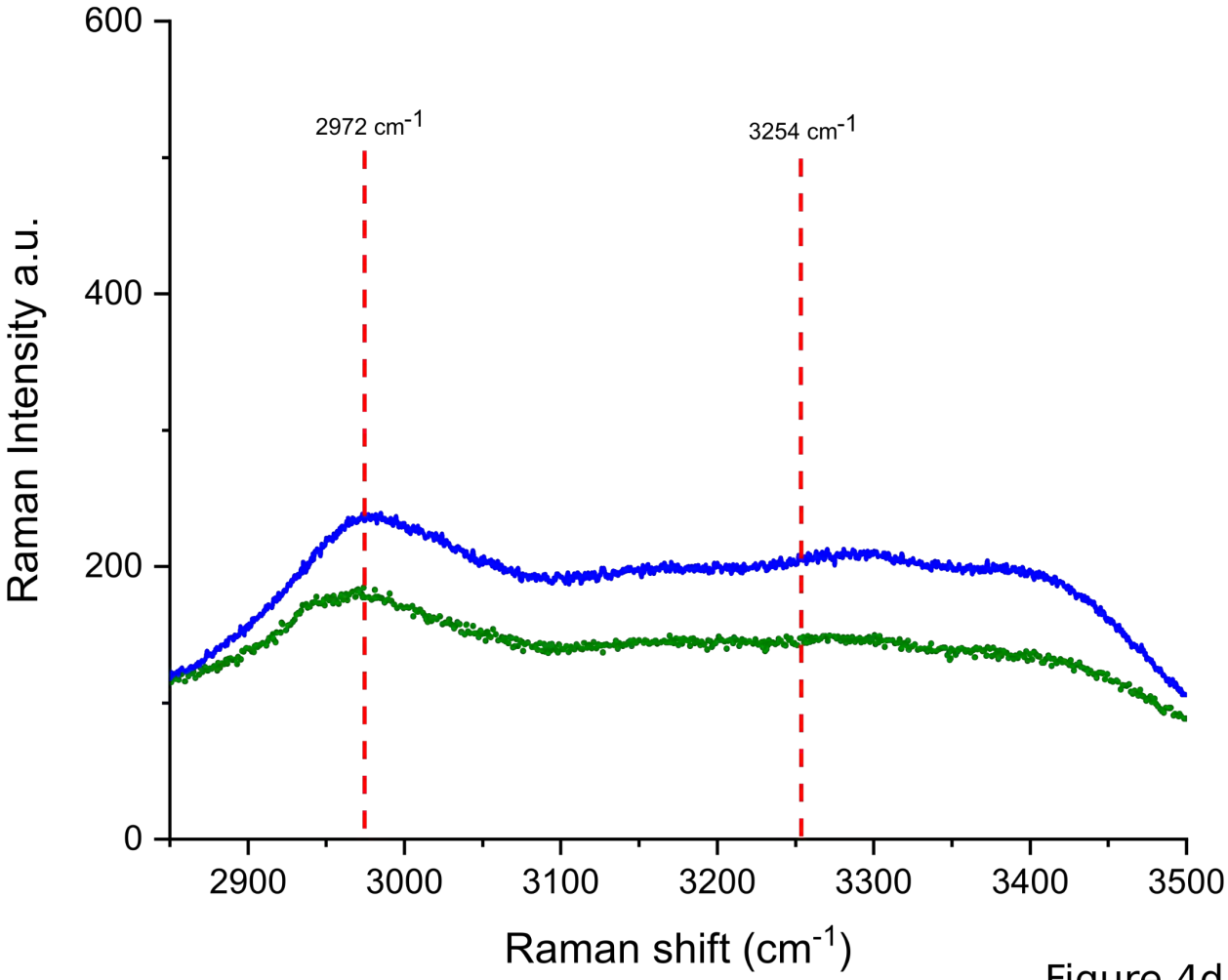


Figure 4d

This is the peer-reviewed, final accepted version for American Mineralogist, published by the Mineralogical Society of America.
The published version is subject to change. Cite as Authors (Year) Title. American Mineralogist, in press.
DOI: https://doi.org/10.2138/am-2022-8106. http://www.minsocam.org/

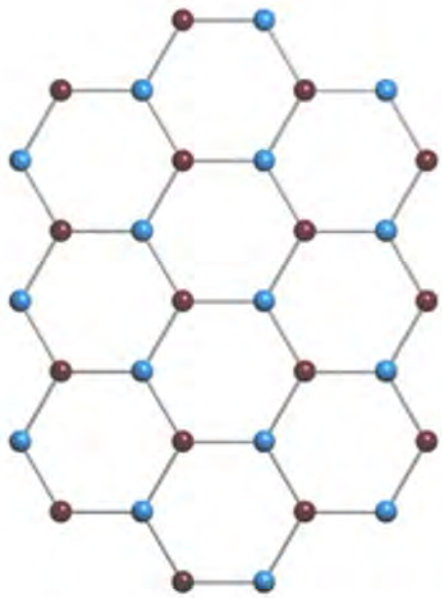

$CaC(1)O_3$ layers
with **hcb** topology

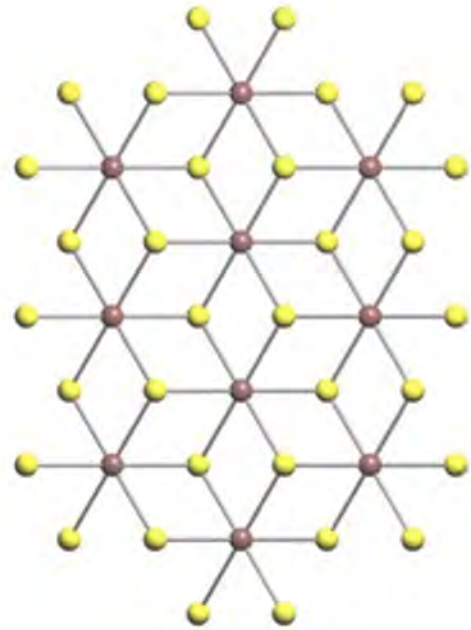

$Na_2C(2)O_3$ layers
with **kgd** topology

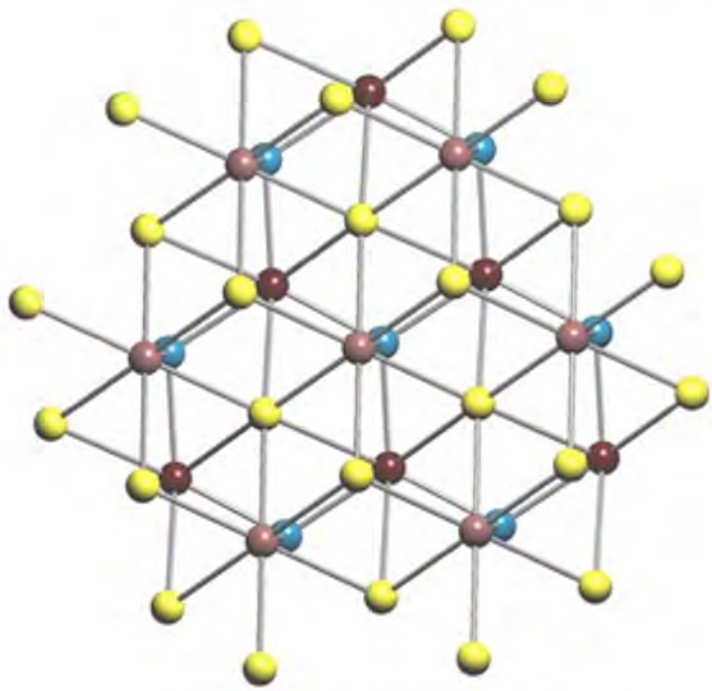

crystal structure of nyerereite
with 5,6,8,9T2 topology

Figure 5

This is the peer-reviewed, final accepted version for American Mineralogist, published by the Mineralogical Society of America.
The published version is subject to change. Cite as Authors (Year) Title. American Mineralogist, in press.
DOI: https://doi.org/10.2138/am-2022-8106. http://www.minsocam.org/

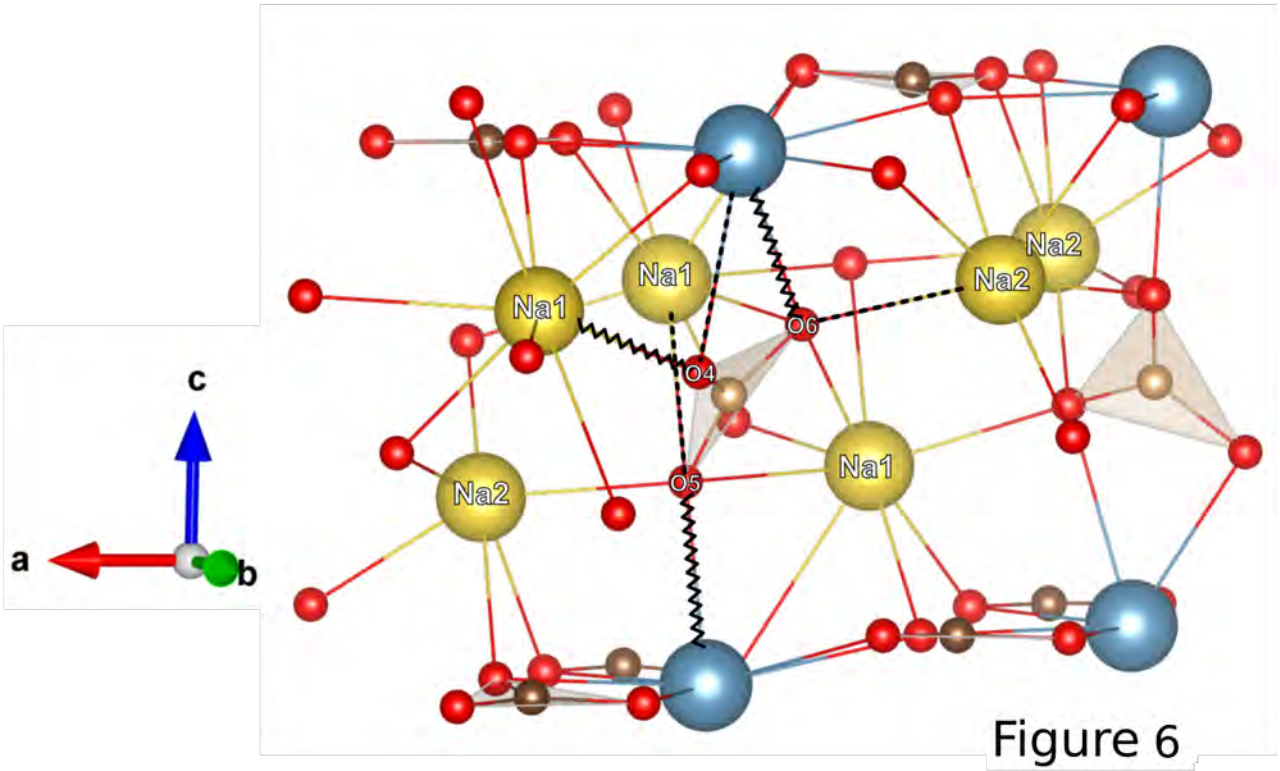


Figure 6

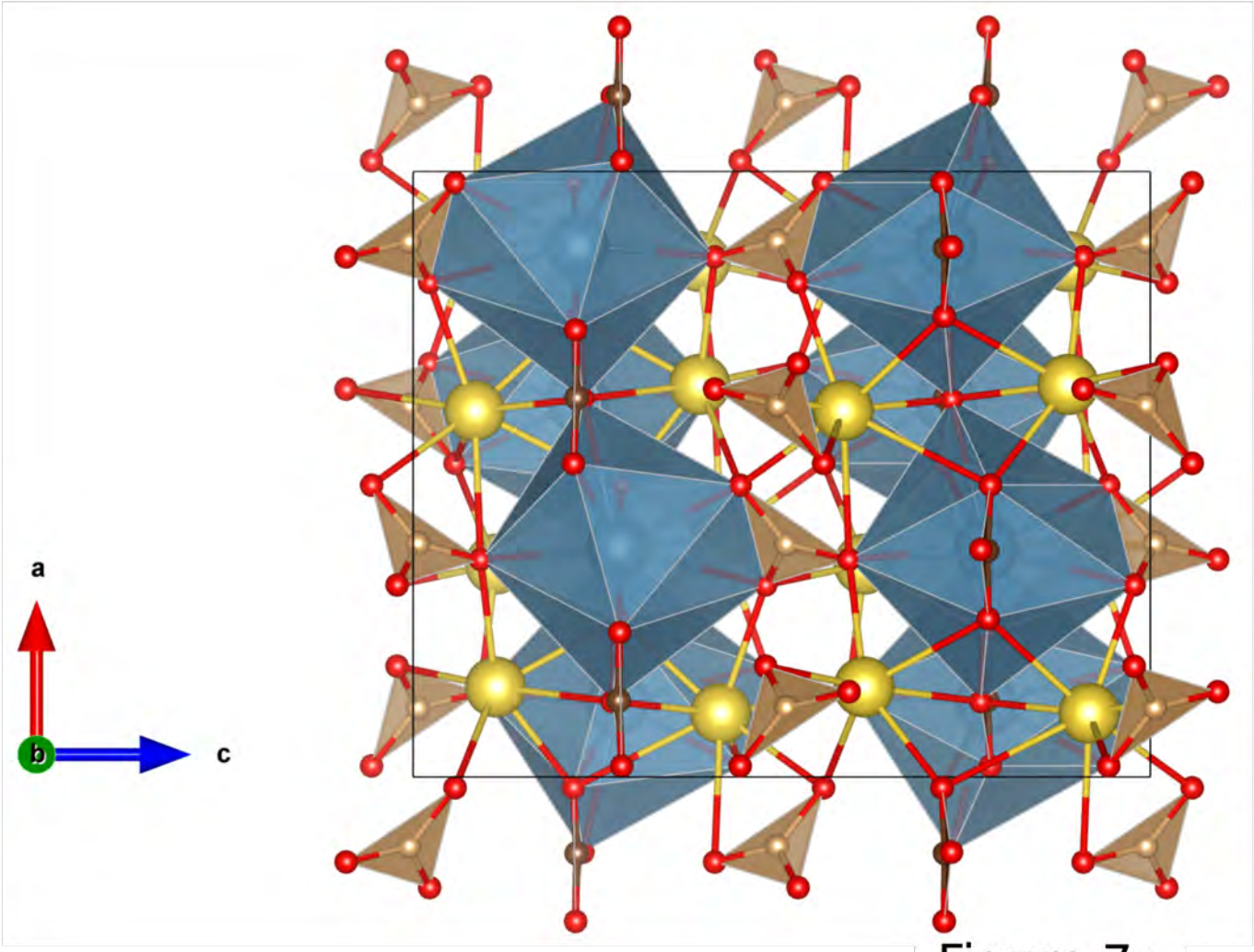


Figure 7a

This is the peer-reviewed, final accepted version for American Mineralogist, published by the Mineralogical Society of America.
The published version is subject to change. Cite as Authors (Year) Title. American Mineralogist, in press.
DOI: https://doi.org/10.2138/am-2022-8106. http://www.minsocam.org/

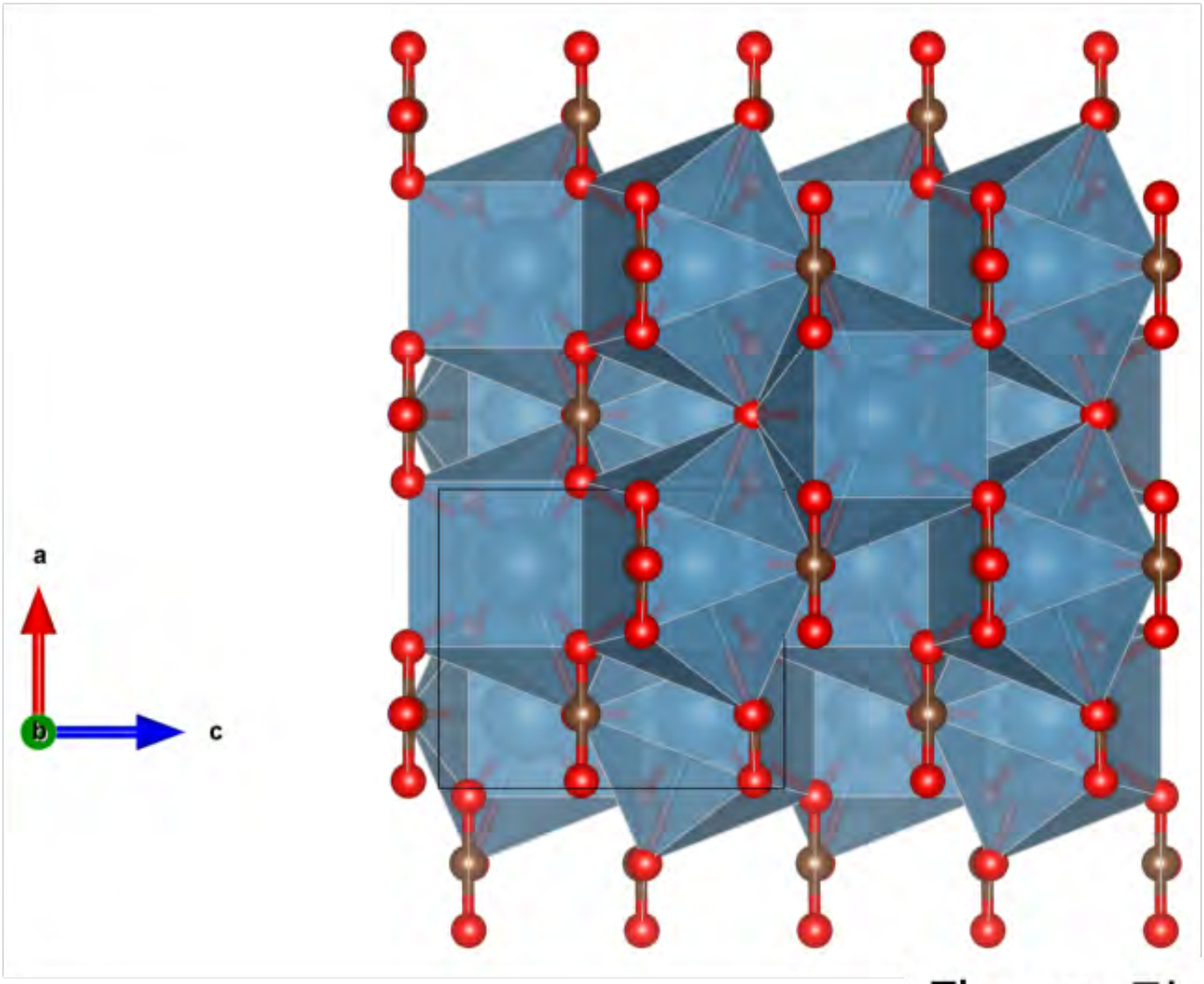


Figure 7b